Submarine Paleoseismology Based on Turbidite Records

Chris Goldfinger

College of Oceanic and Atmospheric Sciences, Oregon State University, Corvallis, Oregon 97331; email: gold@coas.oregonstate.edu

Annu. Rev. Mar. Sci. 2011. 3:35–66

First published online as a Review in Advance on October 27, 2010

The *Annual Review of Marine Science* is online at marine.annualreviews.org

This article's doi: 10.1146/annurev-marine-120709-142852

1941-1405/11/0115-0035$20.00

Keywords

subduction zones, litho-stratigraphic correlation, earthquake recurrence history, turbidites, earthquakes

Abstract

Many of the largest earthquakes are generated at subduction zones or other plate boundary fault systems near enough to the coast that marine environments may record evidence of them. During and shortly after large earthquakes in the coastal and marine environments, a spectrum of evidence may be left behind, mirroring onshore paleoseismic evidence. Shaking or displacement of the seafloor can trigger processes such as turbidity currents, submarine landslides, tsunami (which may be recorded both onshore and offshore), and soft-sediment deformation. Marine sites may also share evidence of fault scarps, colluvial wedges, offset features, and liquefaction or fluid expulsion with their onshore counterparts. This article reviews the use of submarine turbidite deposits for paleoseismology, focuses on the dating and correlation techniques used to establish stratigraphic continuity of marine deposits, and outlines criteria for distinguishing earthquake deposits and the strategies used to acquire suitable samples and data for marine paleoseismology.

1. INTRODUCTION

Offshore and lacustrine records offer the potential of good preservation, good spatial coverage, and long temporal span. Marine deposits offer opportunities for stratigraphic correlation along the source zone, something typically more difficult with land paleoseismology. Stratigraphic correlation methods, widely used in the petroleum industry, are mature and have potential to address source zone spatial extent and fault segmentation. Marine records may be quite long and can be used to examine recurrence models, fault interactions, clustering, and other phenomenon, commonly limited on shore by short temporal records. High-resolution subsurface mapping allows characterization and correlation with core samples to delineate the spatial extent of mass transport deposits and turbidites. Marine deposits also have some disadvantages, primarily because marine earthquake deposits are secondary evidence of rupture and must be distinguished from similar deposits generated by other processes. Specific tests of earthquake origin may be made on the basis of regional correlation, synchronous triggering, sedimentological criteria, comparison with onshore and historical records, or a combination of these.

The classic paper by Heezen & Ewing (1952) demonstrated that offshore earthquakes can trigger turbidity currents. The triggering of turbidity currents and landslides from submarine canyons, shelf edges, and seamount edifices is becoming reasonably well known. These events can be dated and correlated in the marine environment, providing long, continuous records that also serve as good evidence for spatial continuity.

The use of secondary evidence such as landslides and turbidites adds some complexity to this aspect of paleoseismology. The techniques do not use fault outcrops, because the faults are inaccessible, and must demonstrate that the deposits are uniquely generated by earthquakes and not some other natural phenomenon. Nevertheless, these problems can be overcome, and the techniques can be powerful tools for deciphering the earthquake history along an active continental margin. In recent years, turbidite paleoseismology has been attempted in Cascadia (Adams 1990; Blais-Stevens & Clague 2001; Goldfinger et al. 2003a,b; Goldfinger et al. 2007, 2008, 2010), Puget Sound, Washington (Karlin & Abella 1992; Karlin et al. 2004), Japan (Inouchi et al. 1996, Nakajima 2000, Nakajima & Kanai 2000), the Mediterranean (Kastens 1984, Anastasakis & Piper 1991, Nelson et al. 1995), the Dead Sea (Niemi & Ben-Avraham 1994), northern California (Field et al. 1982; Field 1984; Garfield et al. 1994; Goldfinger et al. 2007, 2008), Lake Lucerne (Schnellmann et al. 2002), Taiwan (Huh et al. 2006), the southwest Iberian margin (Gracia et al. 2010), the Chile margin (Blumberg et al. 2008, Völker et al. 2008), the Marmara Sea (McHugh et al. 2006), the Sunda margin (Patton et al. 2010), and even the Arctic Ocean (Grantz et al. 1996). Results from these studies (reviewed in Goldfinger 2009) suggest the turbidite paleoseismologic technique is evolving as a useful tool for seismotectonics.

2. DATING METHODS AND STRATEGIES

2.1. Radiometric Dating

The most common technique used to date submarine events is to date calcareous microfossils, most commonly planktic foraminifera, using accelerated mass spectrometry (AMS) ^{14}C techniques. Samples are typically taken below each turbidite because the boundary between the top of the turbidite tail and the hemipelagic sediment is gradational and thus difficult to identify reliably. Bioturbation is also commonly more intense at the upper boundary (Goldfinger et al. 2008, 2010) (**Figure 1**). Sediment samples are taken to avoid visible deformation and friction drag along the core walls. Computed tomography (CT) imagery can be used to improve sample locations by

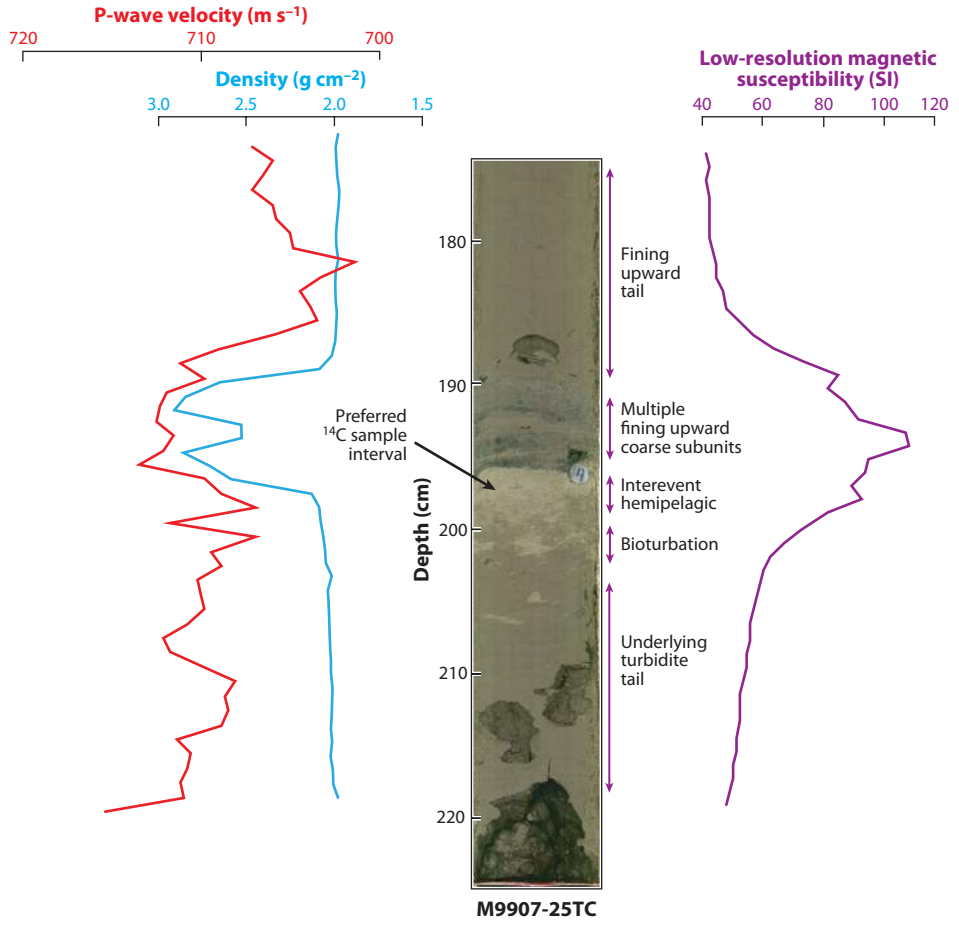

Figure 1

Detail from Cascadia core M9907-25TC; event T4 is shown. Turbidite tail/hemipelagic boundary is commonly distinct visually and variably disturbed by bioturbation. Although turbidite bases can be erosive, dating was done from planktic foraminifers in the upper hemipelagic, being the least problematic option. Typical sample location is shown, with a small gap above the sample. Erosion was evaluated visually in the cores, by comparison to hemipelagic thickness in nonchannel cores, and by intersite comparisons between multiple cores. P-wave velocity, gamma density, and low-resolution loop magnetic susceptibility are shown.

imaging core deformation, bioturbation not visibly apparent, and subtle stratigraphic intervals (**Figure 2**). AMS methods can make use of as little as an ~1-mg carbon sample. Sensitivity tests for species-specific biases and other techniques are presented in Goldfinger et al. (2007, 2010).

All radiocarbon ages must be calibrated to account for variability of carbon isotopes in the atmosphere. Marine ages have several additional complications, most importantly the reservoir correction. This value, representing the age of the seawater in which the datable organisms lived, is a spatially varying value specific to the locality of interest (e.g., Hughen et al. 2004). The published value is commonly derived from paired shell/wood dates that difference coeval marine and terrestrial organisms. The known values are almost exclusively from the twentieth century, though it is known that these values change through time (i.e., Kovanen & Esterbrook 2002). Time

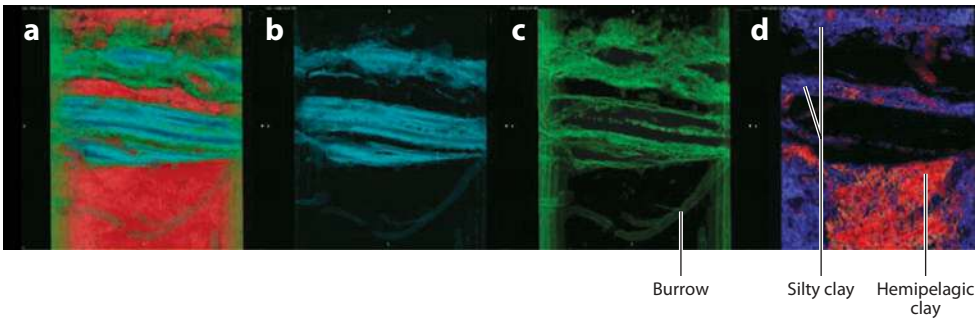

Figure 2

Computed tomography image of a single turbidite with two fining-upward sequences. (*a*) Image coded by density: sand fraction (*blue*), silt (*green*), hemipelagic clay (*red*). (*b*) Sand fraction only. (*c*) Silt fraction only. (*d*) Clay fraction with expanded density differentiation distinguishing between hemipelagic sediment (*red*) of slightly lower density than the upper two silty mud bands (*purple*) that are both part of the turbidite sequence. Differentiation and precise quantification of hemipelagic intervals via imagery and other techniques are critical to core age models, the differentiation of single and multiple events, and the identification of upper boundaries for dating.

variation of the reservoir age is usually ignored for older samples because little data on the time history are available (Stuvier et al. 1998). Some efforts to construct time-space variant reservoir models have been made (e.g., Kovanen & Easterbrook 2002, Fairbanks et al. 2005, Bondevik et al. 2006, Hughen et al. 2006, Schimmelmann et al. 2006). Goldfinger et al. (2010) have developed a model for the Holocene of the Cascadia region and have applied this curve to marine ages along the Cascadia margin. This model makes use of benthic-planktic pairs and onshore-offshore earthquake pairs to construct the model. Globally, more work on reservoir models is needed to improve the accuracy of marine ^{14}C ages.

Because the sedimentation rates in the deep sea can be relatively stable over periods of interest to paleoseismology, radiometric ages can be corrected for such factors as basal erosion, sample offset from the event of interest, and sample thickness. These corrections, detailed in Goldfinger et al. (2010), attempt to bring the age close to the age of deposition of the turbidite.

Basal erosion is a concern when dating landslides or turbidites below their bases. In the case of landslide deposits, it may be advantageous to date material directly above the deposit as it is both easier to sample and lacks the erosion concern. One can mitigate the basal erosion problem to some extent by avoiding obviously eroded intervals, though erosion cannot always be detected and quantified. Another technique is to assess thickness variations among a local group of cores, with the assumption that erosion is likely the primary cause of such variability. Missing section can be estimated from the difference between the thickest and the other intervals (Goldfinger et al. 2008, 2010; Guitierrez-Pastor 2010). This method obviously underestimates erosion in the case in which all intervals are eroded.

Goldfinger et al. (2010) compared the total deposition of hemipelagic sediment in nonturbidite interchannel cores in Cascadia, finding it comparable to the erosion-corrected thickness totalled from channelized turbidite cores, further suggesting that, at least in this case, undetected basal erosion is minor. Turbidity currents, though turbulent and fast-moving, travel over a very slowly moving bottom boundary layer (Stacey & Brown 1988), partially insulating the relatively cohesive seafloor sediments from the high-velocity current. This occurs much less in proximal canyon sites, where significant erosion is commonly evident (Goldfinger et al. 2010) but may dramatically reduce erosion at more distal sites.

Goldfinger et al. (2010) show the improvement in both regional consistency of event ages and a close temporal correlation to onshore ages along the Cascadia margin, based on correcting for erosion where indicated. The erosion and other sample or offset corrections to the radiocarbon ages can be made iteratively until a convergence of the data set is achieved, because the radiocarbon ages control the sedimentation rates but are themselves being corrected (using these rates) in this process.

Radiocarbon ages are typically reported as 1σ or 2σ ranges. However, the probability distribution generated during the calibration process contains more information, and a graphic representation of this distribution is presently the best way to represent a radiocarbon age. The graphic density function may illustrate multiple density peaks, or lack thereof, and thus informs the reader of the best way to represent the age information (Niklaus et al. 1994). Usually single-point representations of ^{14}C ages are not particularly good due to the possibility of multiple peaks (Telford et al. 2004); however, the probability peak or mode may be useful where marine ages are constrained by sedimentation rates and multiple peaks are not a factor (Blaauw et al. 2003, Walanus 2008).

To develop age models or model undated events, the boundary between the gradational turbidite tail and the overlying hemipelagic sediment must be determined as precisely as possible. This can be difficult because the differences between the very-fine-grained turbidite tail and the overlying hemipelagic sediment may be nearly nonexistent and may be region specific. In some cases, turbidites may have obvious boundaries that are clearly visible to the unaided eye (Goldfinger et al. 2008, 2009). For many other regions, the problem is more difficult. Many attempts have been made to find universal methods for defining this boundary, including clay fabric orientation (O'Brien et al. 1980, Azmon 1981), color (Rogerson et al. 2006), hydraulic sorting of microfossils (e.g., Brunner & Ledbetter 1987), XRF and XRD (e.g., Bernd et al. 2002), CT methods (Patton et al. 2010), grain size (the most common method, i.e., Brunner & Ledbetter 1987, Joseph et al. 1998, St-Onge et al. 2004), and resistivity, among others. Some experimentation may be needed to find acceptable criteria for a given locality.

2.2. Bayesian' Analysis

One of the most powerful tools available for analysis of radiocarbon data is analysis of multiple criteria for the age of an event using Bayes' theorem. This allows the combination of disparate sources of age information to define a probability function for an event or stratigraphic age. These constraints can be combined with calibration for the radiocarbon ages. OxCal is one such package that includes multiple methods to allow for the use of multiple ^{14}C ages and constraints such as sedimentation rate to constrain radiocarbon ages (Ramsey 1995, 2001). External constraints may include (*a*) the time represented by sediment deposited between events; (*b*) historical information; (*c*) stratigraphic ordering; (*d*) events or horizons dated with multiple samples; and (*e*) other external stratigraphic constraints such as dated ashes, pollen, or other biostratigraphic markers (Biasi et al. 2002, Goldfinger et al. 2007). Event ages can also be estimated where interevent sedimentation thicknesses and rates are well known. Ages corrected or estimated using sedimentation rates include some unavoidable issues, such as the circularity resulting from calculated sedimentation rates that are also dependent on the radiocarbon ages. Ages are also affected by basal erosion unless varves or other independently derived rates are available (e.g., Kelsey et al. 2005). However, this problem may be mitigated by computing the rates and ages iteratively until a convergence is reached (Heath 2002). **Figure 3** shows an example of constraining an event age with stratigraphic control.

2.3. Event Ages and Potential Biases

The question of how well the radiometric ages from marine deposits represent earthquake ages is complex. Event ages onshore commonly represent maximum or minimum ages when dated using sample material below or above the event, respectively, bracketing the event age (e.g., Nelson et al. 2006, 2008). The sample materials are commonly detrital, and thus certain to be of a different age (usually older) than the age of deposition. Marine ages have advantages in that they may include attempts to correct known biases based on continuous sedimentation, and the difference between death and deposition is small for marine microfossils compared with some of the wood, plant, or charcoal materials used onshore. The sedimentation rate corrections, erosion analyses, and OxCal

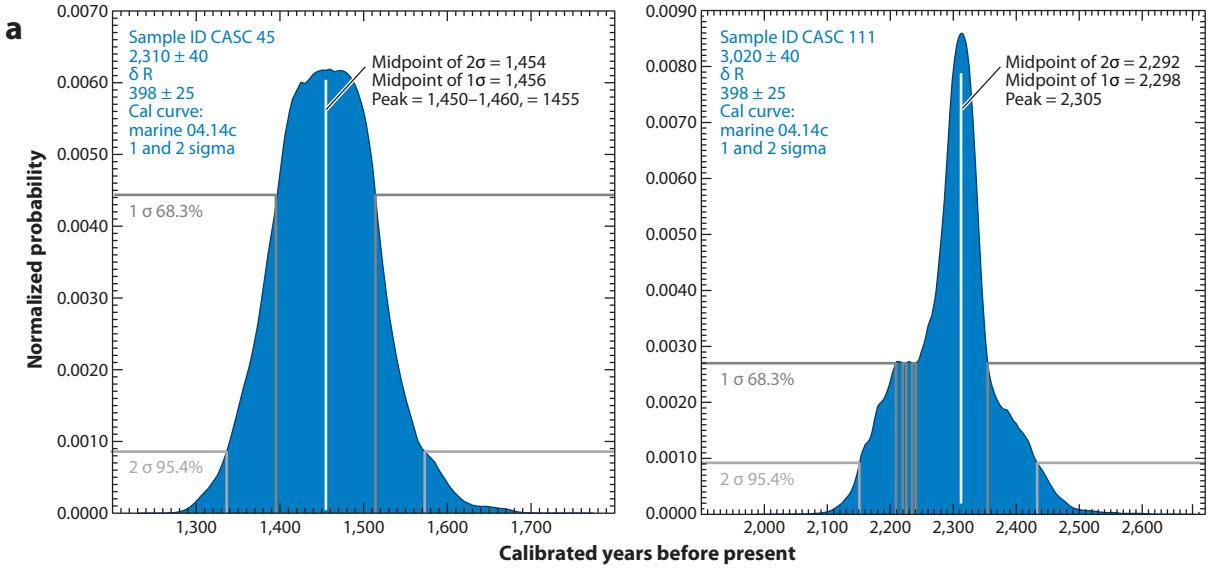

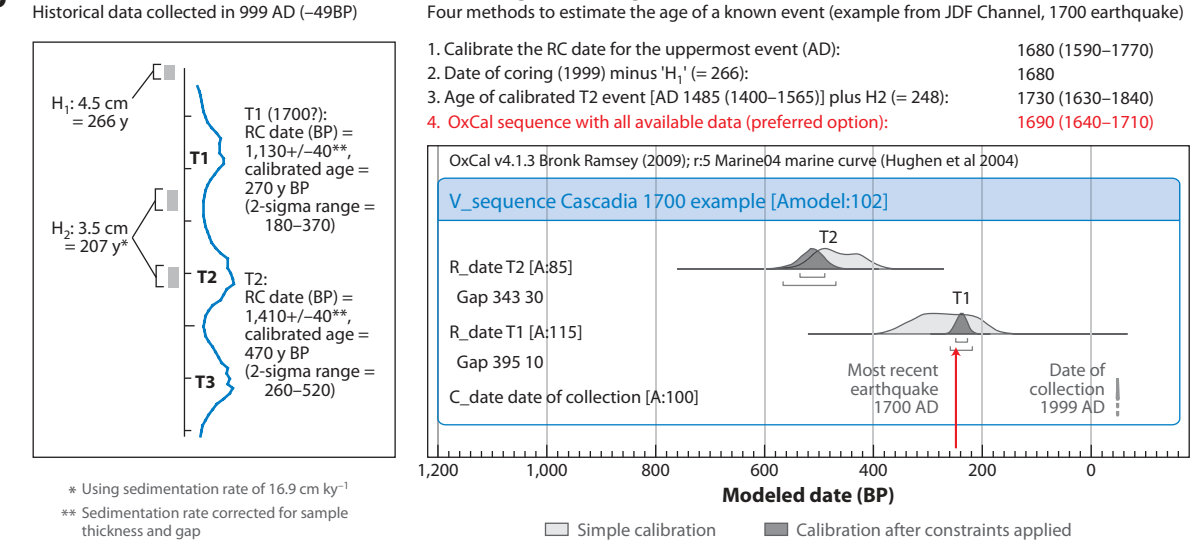

analyses using hemipelagic interval constraints are designed to model event ages by attempting to remove these biases. Goldfinger et al. (2010) give examples of testing these methods against events of known age with good results. Biases will always remain, as in the case of undetected erosion and bioturbation, but dating of multiple instances of the same events at one or multiple sites may address these remaining problems. An example of a space-time diagram relating onshore and offshore radiocarbon data is shown in **Figure 4**.

2.4. Short-Half-Life Radiometric Dating

Activity rates of Pb210 can be used either to determine the age of the uppermost sediment or to determine that the uppermost material was older than the maximum typical age when Pb210 reached background levels (~150 years; Robbins & Edgington 1975). The logarithmic decay of Pb-210 begins below the shallow, low-density mixed layer, and most Pb-210 analyses assume that the mixed layer is entrained in any turbid flow and completely removed from the record we observe in sediment cores. This apparently does not present a significant problem, as there is apparently little or no time lost by removing the mixed layer as its Pb-210 age is constant and near zero on the seafloor prior to the rapid deposition of turbidites (Nittrouer 1978).

Cs-137 may be used for the very youngest materials. The half life of Cs-137 is 30.3 years. Its presence is due to the atmospheric testing of nuclear devices during the 1950s and early 1960s (Schuller et al. 1993, 2002). Since that time, there has been no Cs-137 released to the atmosphere following the termination of atmospheric nuclear testing except for very recent small releases. The maximum value is associated with the high fluxes of Cs137 between 1962 and 1965, with the peak value commonly assumed to be 1963 $\pm$ 2 years, giving a sharp peak that can be used to constrain sedimentation rates and calculate ages of post-bomb strata. In some settings including marsh peat and organic materials, Cs-137 has been shown to be mobile and not useful for dating.

2.5. Bioturbation and Its Effect on Radiocarbon Dating of Interseismic Hemipelagic Sediments

Bioturbation can have serious effects when attempting to precisely date submarine events. Some attempts have been made to test the dependency of vertical rates of mixing of microfossils during

Figure 3

(*a*) Calibration examples. Samples Cascadia (CASC) 45 and CASC 11 are illustrated, calibrated with Calib 5.02 and showing the probability density function (PDF) and 1 σ and 2 σ ranges. The left panel reflects many samples in our data set, where the peak PDF, mode, and midpoint of 1 σ and 2 σ ranges were indistinguishable, as shown by the vertical lines indicating these parameters. Right panel shows a skewed peak and minor multimodal peak. For samples with this type of distribution, minor modes were rejected and the peak was selected when point representation of the age was required. More complex cases with multimodal peaks were constrained with prior data when possible, as illustrated in (*b*). Where prior constraints were not available, the midpoint of the 2 σ range was used. (*b*) Example of OxCal methods, using the well-constrained AD 1700 earthquake and associated paleoseismic data onshore and offshore. The age of this event is well known through ^{14}C, tree ring data, and Japanese historical records (Atwater et al. 1997, 2003; Jacoby et al. 1997; Satake et al. 2003). The left panel shows the hemipelagic (H) data determined from visual observation, physical property data, smear slide mineralogy, and X-radiography. H data are then input to OxCal, with raw ^{14}C ages converted to time via sedimentation rate curves developed for each site. Oxcal modeled gaps include sample interval, erosion if any, and basal gap. Right panel shows four ways to calculate the age of the 1700 earthquake, as determined from historical data, with the preferred method being the use of underlying and overlying hemipelagic intervals (none for this example). This method commonly reduces the ambiguities inherent in radiocarbon dating where PDFs have multiple peaks or broad distributions due to the slope or complexity of the calibration curve. In this example, the overlying ~300 years of hemipelagic sediment in Cascadia restricts the PDF to the earlier of three peaks. Such constraints are typically not as strong for events deeper in the core section, because the present day upper boundary layer is absolute for the uppermost layer. Abbreviation: JDF, Juan de Fuca.

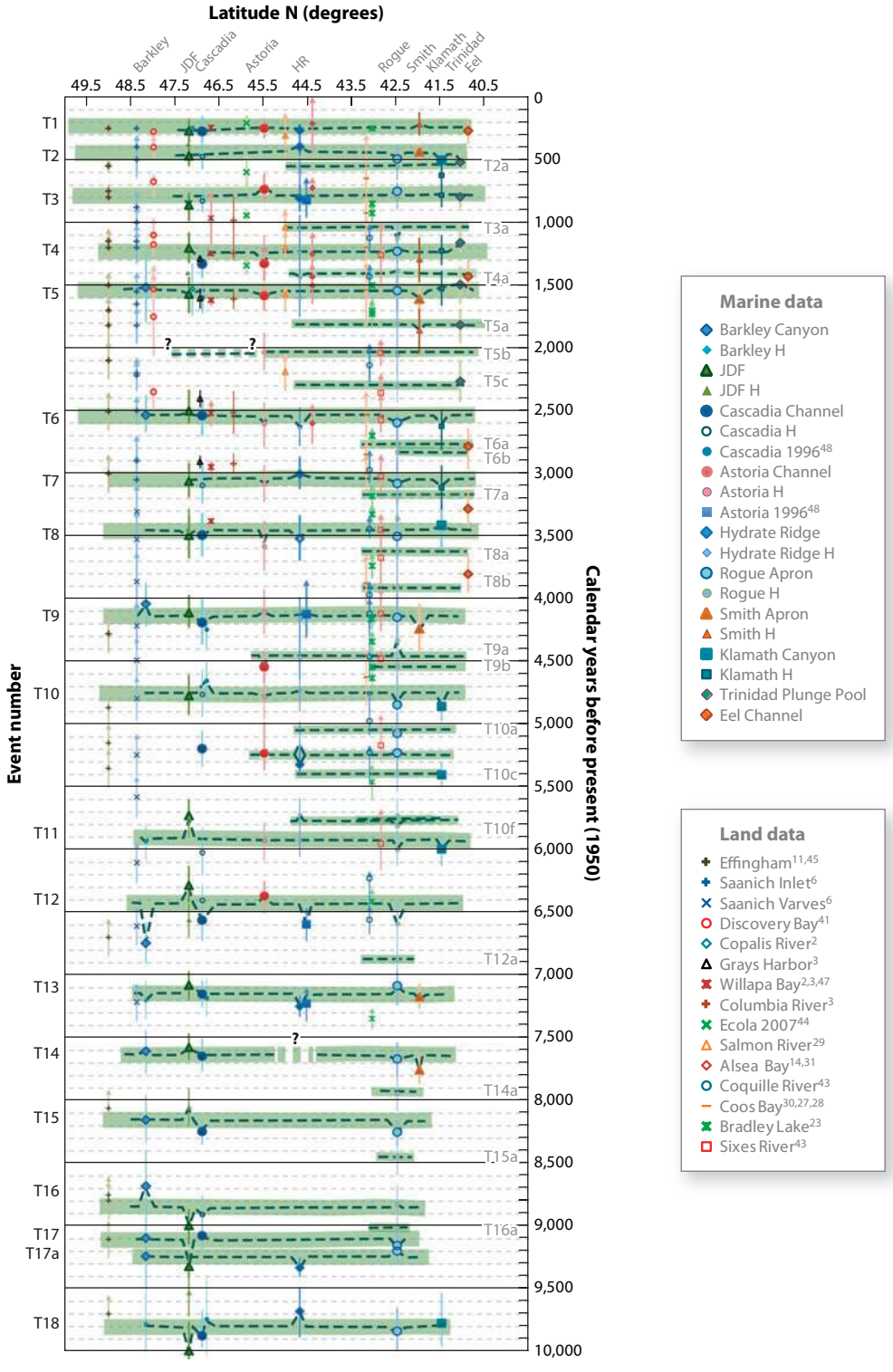

bioturbation. Vertical mixing of single species may be dependent on temperature, particle size, and particle shape (Wheatcroft 1992, and references therein). Experimental results from several settings suggest that bioturbation in the deep sea is caused by deposit feeders that preferentially ingest and retain fine particles (Thomson et al. 1988, Wheatcroft 1992, Thomson & Weaver 1994). Relatively large particles such as foraminifers are not selected by deposit feeders for retention and apparently are not vertically mixed as much as the finer fractions of material. These results may help explain the surprising consistency observed when dating correlative turbidites (Goldfinger et al. 2010), despite bioturbated sample intervals, when other variables such as reservoir age, basal erosion, and contamination are minimized.

2.6. Stratigraphic Datums

Tephra layers are common stratigraphic intervals that provide potential for onshore-offshore linkage and age corroboration. In Cascadia, the widespread deposition of ash sourced from the eruption of Mount Mazama provides a clear datum throughout most of the Cascadia Basin system with independent age control. The age of the Mazama eruption is well constrained at 7,627 ± 150 cal BP (Zdanowicz et al. 1999) from Greenland ice cores, and 7,605 ± 29 in lake sediments in British Columbia (calibrated from Hallett et al. 1997). The first turbidite containing the Mazama ash has been dated in five localities, combined with OxCal to derive an event age of 7,130 ± 45, approximately 500 years after the Mazama eruption (Goldfinger et al. 2010). Earlier work identified this Mazama ash–bearing turbidite as the thirteenth event down from the surface in many Cascadia Basin cores (Adams 1990; Goldfinger et al. 2003a,b). Subsequent work demonstrated that in a single channel system linked directly to Mount Mazama, the Mazama ash first appeared in fourteenth margin–wide turbidite. The age of this event is 7,620 ± 60, identical to the onshore ages, and Goldfinger et al. (2010) interpret this event to have occurred in the same year as the Mazama eruption, revealing the age precision possible under ideal conditions (**Figure 5**).

Similar stratigraphic control can be found in other settings. Along the Sumatran margin, multiple tephras with good elemental fingerprints constrain the turbidite stratigraphic sequence (M. Salisbury, pers. commun.). Similarly, turbidite ages have been constrained by tephra markers in Lake Biwa, Japan (Inouchi et al. 1996), where 20 turbidites were correlated to the historical record of earthquakes, and their ages calculated using sedimentation rates above historical tephra markers. Other records tied to tephras have been reported in the Japan Sea (Nakajima & Kanai 2000, Abdeldayem et al. 2004), lakes in Tierra del Fuego (Waldmann et al. 2008), the Ionian Sea (Ryan & Heezen 1965), the Ulleung Basin in Korea (Bahk et al. 2004), and elsewhere. Similarly, Noda et al. (2008) used a tephra marker to help support the dating and correlation of turbidite stratigraphy on a fan setting in the Kurile Trench.

Figure 4

Space-time diagram for the Cascadia margin, showing Holocene marine radiocarbon data and stratigraphic correlations. Larger filled symbols are marine ^{14}C ages; smaller filled symbols are ages calculated using hemipelagic (H) layers. Marine data plotted as 2σ midpoints with 2σ root mean square ranges. Dashed lines indicate stratigraphic correlation of the turbidite data, which show deviations from the preferred age range where correlation overrules individual ^{14}C ages. Up arrows are shown for marine data where site-wide erosion suggests a maximum age. Southern Cascadia events of reduced spatial extent are shown with thinner dashed lines. Green bars are best-fitting offshore-onshore age trends for Cascadia earthquakes. High-precision land data are included. Down arrows indicate minimum ages as published (land only). Two-sided arrows are shown where maximum and minimum ages have been averaged (land sites only). Marine ^{14}C data, and onshore data and numbered sources, are taken from Goldfinger et al. (2010, App. 1 and 2, respectively), and superscript numerals shown in Land Data are keyed to references therein. Abbreviation: JDF, Juan de Fuca.

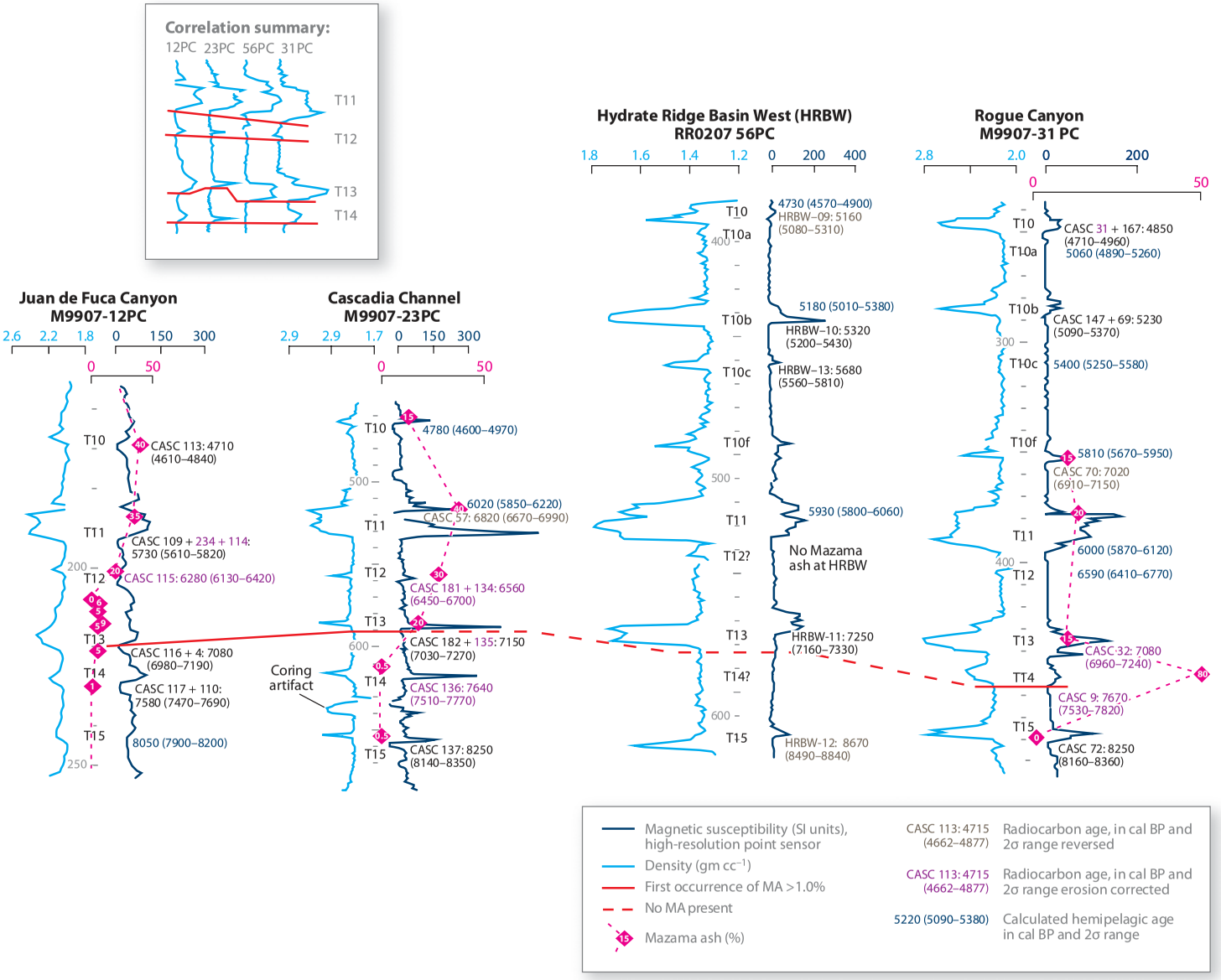

3. DISTINGUISHING EARTHQUAKE- AND NON-EARTHQUAKE-TRIGGERING MECHANISMS

3.1. Possible Triggering Mechanisms

Triggering events for turbidity currents may include (*a*) earthquakes, (*b*) volcanic explosions, (*c*) tsunami, (*d*) subaerial landslides into the marine environment, (*e*) storm wave loading, (*f*) tidal surges and other currents, and (*g*) hyperpycnal flow. These primary triggers are distinguished from factors that may destabilize slopes through longer-term processes such as sediment self-loading, gas hydrate thermal destabilization, sea-level change, shelf edges destabilized by groundwater input, volcanic seamount or island edifice destabilization, tectonic folding/tilting, and other factors. Most destabilizing factors still require another trigger; for example, the Storegga slide occurred as a result of the massive deposition of glacial sediments and associated gas hydrate disassociation that destabilized the local stratigraphy (e.g., Solheim et al. 2005) but was most likely triggered by an earthquake (Bryna et al. 2005).

If turbidites from these sources are inherently difficult to distinguish from one another, how can an earthquake-triggered turbidite be identified? An equally important question is whether environments can be found that favor preservation of earthquake deposits while disfavoring other deposits? Essentially, two methods can be used to differentiate earthquake-generated turbidites from those originating from other processes: sedimentological examination, and tests for synchronous triggering that can eliminate deposits with nonearthquake origins. Both of these methods may be augmented by a historical earthquake record if available.

3.2. Synchronous Triggering

Two primary characteristics that can be distinguished from a regional set of sediment cores are synchronous deposition and spatial extent. When turbidite deposits can be positively correlated among widely spaced sites, synchronous deposition can be established or inferred. If the spatial extent exceeds that reasonable for other mechanisms, then earthquake triggering is likely. Virtually all studies that make the linkage between earthquake triggering and turbidites invoke this test in some fashion, including those that also use sedimentological criteria (Adams 1990; Gorsline et al. 2000; Nakajima & Kanai 2000; Goldfinger et al. 2003b, 2007, 2008). Because absolute dating techniques cannot demonstrate synchronous triggering and deposition, these tests require other methods to test for this characteristic.

3.3. Numerical Coincidence and Relative Dating Tests

In his synthesis of Cascadia Basin turbidite events, Adams (1990) offered two tests for synchronous deposition. He observed that in several canyons feeding into a confluence off the Washington

Figure 5

Mazama ash (MA) correlation in Cascadia (CASC) Basin. Four cores are shown, including representatives from Juan de Fuca Canyon, Cascadia Channel, Hydrate Ridge Basin, and Rogue Apron systems. The first appearance of Mazama ash in Cascadia Basin cores (*solid red line*), and a very subdued mud turbidite in Hydrate Ridge Basin core in the stratigraphic position of T14 (*dashed red line*), are shown. Percentage glass in the sand fraction of corresponding turbidites (*red diamonds*) is also shown. Inset shows correlation details of magnetic susceptibility curves closely spaced for comparison. Regionally, the first appearance of ash is in T13, but its first appearance in Rogue Apron is in T14, ~500 years earlier. No ash is found in Hydrate Ridge Basin, confirming the lack of terrigenous transport into the isolated basin. Abbreviation: HRBW, Hydrate Ridge Basin West.

margin, cores contained 13–14 turbidites above a regional tephra, the Mazama ash. Below the confluence, cores in the main Cascadia Channel also contained 13 turbidites (**Figure 6**). He reasoned that these events must have been synchronously triggered, because if they had been independently triggered with more than a brief separation in time, cores taken below the confluence should contain from 26–28 turbidites, not 13 as observed. The synchroneity demonstrated by this confluence test is also supported by the similar numbers of events alone, without the existence of the confluence, suggesting either synchronous triggering or a regionally coherent coincidence. Similarly, off the California margin, Goldfinger et al. (2007) used multiple channel confluences along the northern San Andreas fault (NSAF) to show that the stratigraphic sequence remains constant above and below confluences, requiring precise timing of the arrival of the turbidity current. Goldfinger et al. (2010) also observe that the detailed structure of the turbidites also remains constant through confluences in both the Cascadia and NSAF systems. The provenance of the individual pulses was observed to shift along the margin in the NSAF system as different source regions were sampled along strike by adjacent canyons. This observation also precludes the origin of multipulses in the turbidites from being related to multiple tributaries or aftershocks, as these influences are highly variable from one canyon to another.

3.4. Stratigraphic Correlation

Stratigraphic correlation of individual deposits among separated sites offers a straightforward test of event synchroneity. Stratigraphic correlation takes advantage of relatively continuous marine sedimentation in a variety of depositional settings.

3.4.1. Litho-stratigraphic and physical properties correlation. Marine sediment cores are commonly scanned with a multisensor logger that collects gamma density, magnetic susceptibility (MS), P-wave velocity, resistivity, and other parameters. Other parameters may include X-ray fluorescence (XRF), CT density, grain size, color reflectance, and others. Physical property data can do an excellent job of representing the sedimentary units within the core (e.g., Weber et al. 1997a). These parameters are represented as wiggle traces that can be displayed with core imagery and correlated interactively, flattening the turbidite sequences to particular horizons by stretching and squeezing the traces and imagery of cores relative to each other, and using ghost traces to compare the detailed match of wiggle traces from site to site, similar to e-log correlation in the oil industry (McCubbin 1982, Lovlie & Van Veen 1995, Chen et al. 2009). Physical property correlations of this type are also common practice with academic and ODP/IODP cores (e.g., Fukuma 1998) and have recently come into use for paleoseismology (i.e., Schnellmann et al. 2002; Abdelayem et al. 2004; Hagstrum et al. 2004; Iwaki et al. 2003; Karlin et al. 2004; St. Onge et al. 2004; Goldfinger et al. 2008, 2010).

Individual event signatures can be made more robust at a given site by acquiring multiple cores at each site. This reduces the possibility of correlating an unrepresentative example of a given event and allows for assessment of basal erosion and missing tops across the core set. Gamma or CT density and MS data are typically collected on horizontal and vertical axes, respectively, relative to a round core on the scanner track. This yields a good cross-check that signatures of a given interval are not the result of local three-dimensional effects within the core, which are relatively common.

Physical property data are commonly used to correlate local cores, but it is also possible to correlate unique physical property signatures of individual turbidites between more distant sites, and between isolated sites with no physical connection (Schnellmann et al. 2002; Goldfinger et al. 2008, 2010; Patton et al. 2010). These turbidite fingerprints form the basis of along-strike

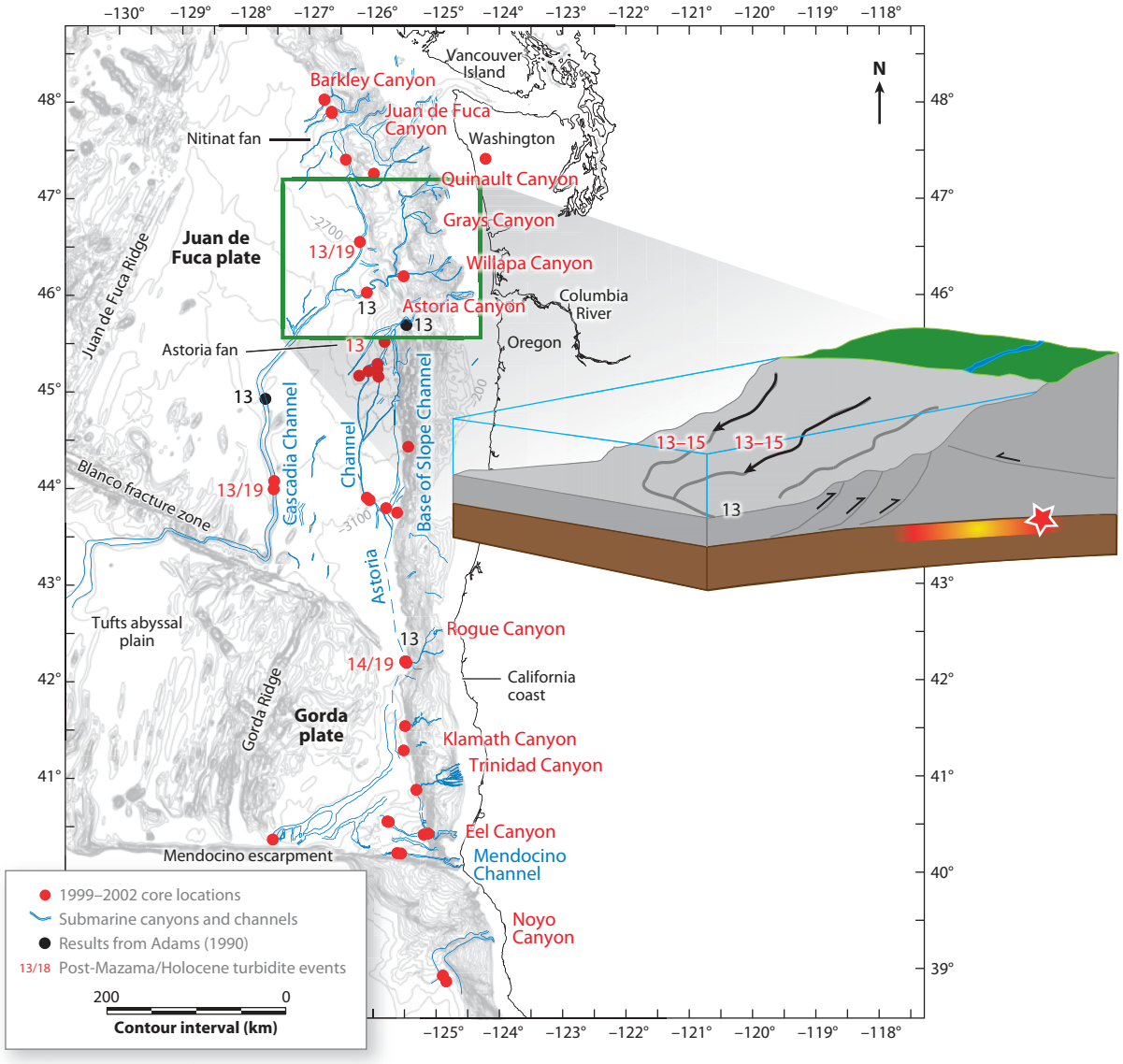

Figure 6

Synchroneity test at a channel confluence as applied where multiple Washington channels merge into the Cascadia Deep Sea Channel (*green square*). The number of events downstream should be the sum of events in the tributaries, unless the turbidity currents were triggered simultaneously. The remarkable similarity of records in northern Cascadia supports the initial conclusion of Adams (1990) that these events are likely of earthquake origin. The number of events present above the Mazama ash remains constant between tributaries and the main stem. The internal structure and number of coarse pulses also remain constant after passage through the confluence.

correlations, closely supported by ^{14}C ages. **Figures 7** and **8** show several representative turbidites, illustrating the multiple fining-upward sequences (Bouma A–C) that compose each turbidite. Typically, these sequences have only one fine tail (Bouma D) associated with waning of the turbidity current. **Figures 7** and **8** show in detail that the MS, density, and grain size trends within each event are closely correlated, allowing the use of high-resolution density and magnetic data as grain size proxies in many cases, though this must be verified with each lithology. In detail, the MS signal is associated with terrestrial silt-sized magnetic minerals, though sand is usually present at the turbidite base (see Stupavsky et al. 1976, King et al. 1982). The sand may be nonmagnetic quartz grains, so the MS peak does not always correlate precisely with a maximum of grain size. Nevertheless, the approximation is reasonable in most cases (and using both density and MS reduces this problem). These fingerprints therefore represent detailed depositional time histories of each turbidite.

The detailed geophysical fingerprinting of turbidites through their grain size proxies has direct implications for synchronous origins of the deposits. Goldfinger et al. (2007, 2008, 2010) and Patton et al. (2010) show that tracking individual deposits through their physical property signatures, combined with stratigraphic details revealed in CT imagery and direct observation, forms the basis of positive correlation. When supported by consistent (though rarely diagnostic) age dates, it is feasible to interpret the deposits as resulting from the same event, establishing synchroneity along strike. The best use of this technique is to examine correlations between sites that have no physical connection, such as slope basin and trench sites, or slope basins isolated from each other and land sources of sediment supply (Goldfinger et al. 2007, 2008, 2010; Patton et al. 2010).

That such grain-size fingerprints exist suggests that triggering mechanisms that produced them, or influences such as hydrodynamics or physiography, must have some commonality, as producing matching grain-size patterns in multipulse turbidites by coincidence is unlikely. The correlative patterns must be reproduced in multiple canyon/channel systems, as well as isolated slope basins with no sources of terrigenous input, and may have no canyon system feeding them. Detailed stratigraphic fingerprinting also provides an extension to the original confluence test of Adams (1990). Goldfinger et al. (2010) observe that turbidites at Juan de Fuca (JDF) and Cascadia channels are among the best correlation series in Cascadia Basin (**Figure 7**), yet Juan de Fuca is upstream and Cascadia is downstream of the Willapa Channel confluence. Not only is the total number of events the same, but the number of coarse fraction pulses remains the same in nearly all cases. This occurs despite the addition of input from Quinault, Grays, and Willapa canyons at the confluence. Patton et al. (2010) make similar observations along the Sumatran margin. The preservation of the individual fingerprints above and below the confluence further supports a synchronous and common origin, which is best attributed to earthquakes.

3.4.2. Seismic stratigraphic correlation. A powerful technique for tracking turbidites is seismic stratigraphy. High-resolution reflection profiles, particularly if collected with a Chirp system

Figure 7

Correlation details from two representative pairs of cores on the Cascadia (CASC) margin. (*a*) Events 8–11 in cores from Juan de Fuca Channel (*left*) and Cascadia Channel (*right*). Left traces are raw gamma density; right traces are magnetic susceptibility. Lithologic logs are also shown. Note correspondence of size, spacing, number of peaks, and trends of physical property traces between these cores. (*b*) Events T10–T14 in Juan de Fuca Channel (*left*) and T10d–T14 in Rogue Channel (*right*). Panel (*a*) cores are part of the same channel system; distance along channel = 475 km. Panel (*b*) cores are in channels that do not meet; separation distance = 500 km. Note that correlation of longer sections with ^{14}C data shows that T10d and T10 do not correlate in (*b*). Similarly, Mazama ash appears in T14, not T13, in the Rogue Apron; see text and **Figure 5** for details.

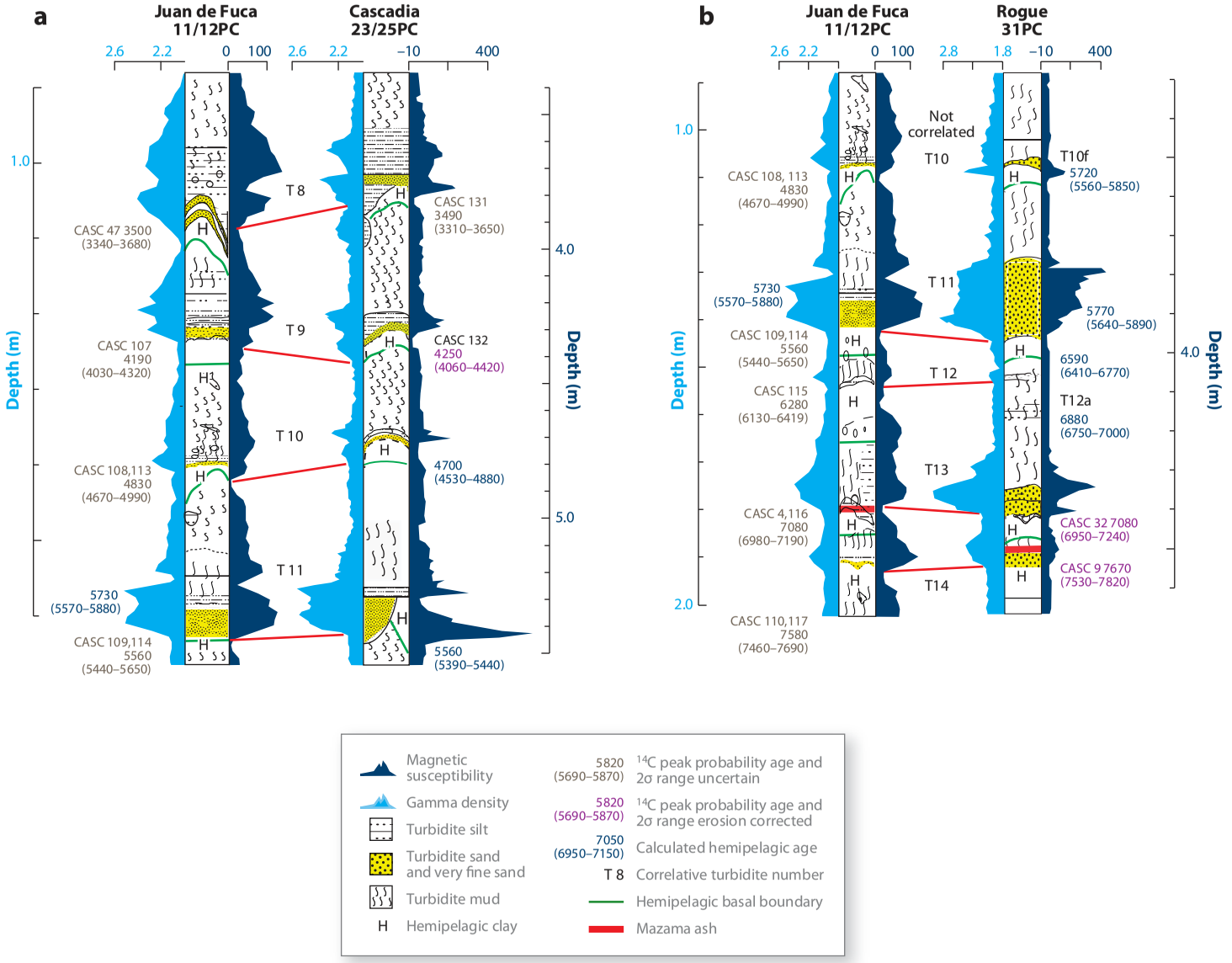

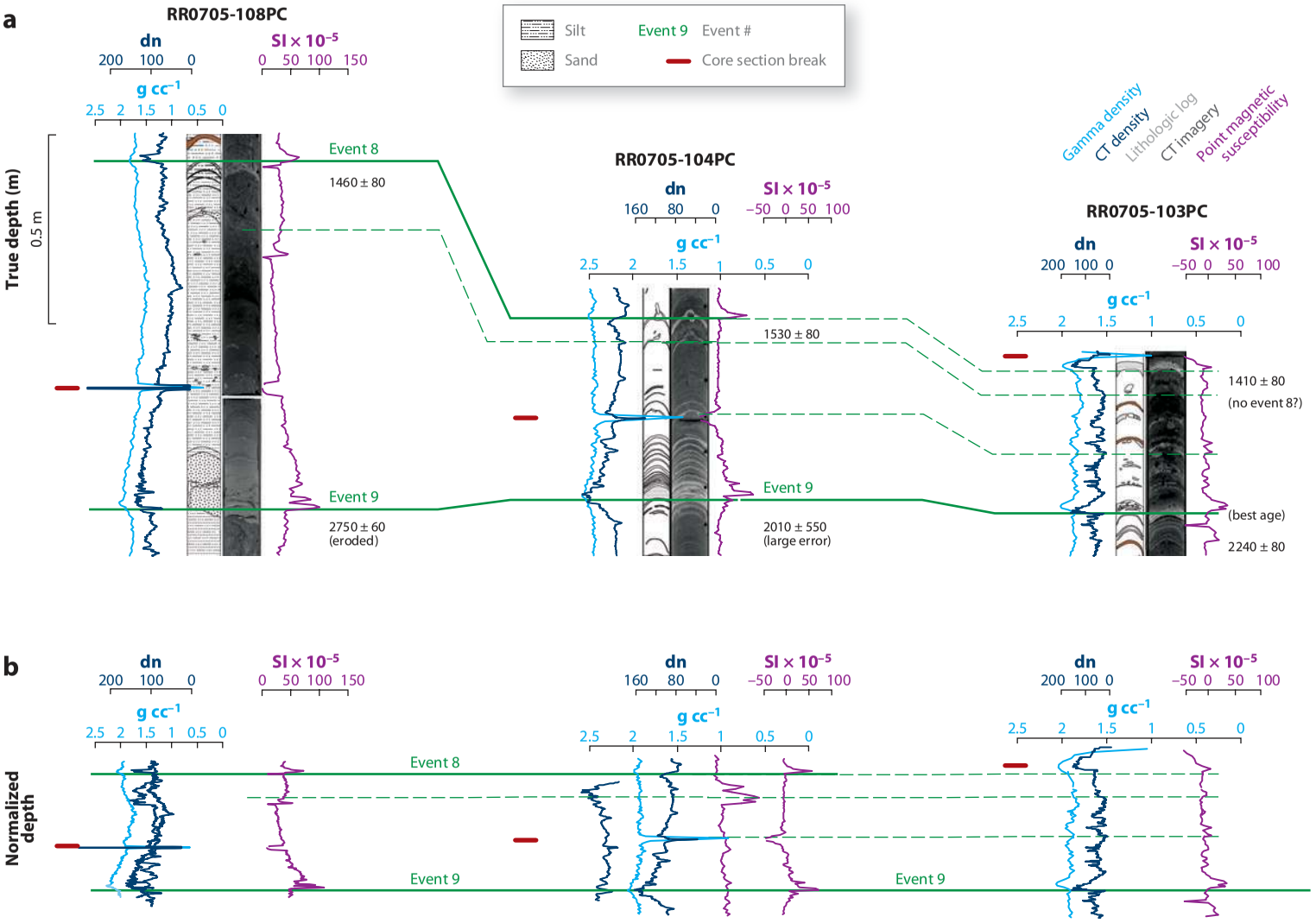

(typically sweeping through ~2–20 kHz), are capable of imaging individual turbidites of 10–25-cm thickness in water depths as great as 4,000–6,000 m (**Figure 9**). Using digital correlation processing in the receiver, the signal-to-noise ratio is improved, and the normally much longer pulse length required in deeper water can be used while retaining good resolution. In other words, the processed pulse length is independent of the transmitted pulse length and is a function of only the swept frequency. With a beam angle of ~20°, scatterers in the water column, and off-axis returns, the resolution is degraded somewhat (Frappa & Pujos 1994).

High-resolution sub-bottom data may be postprocessed to develop depth sections from the SEG-Y time section data. Velocity models may then be constructed for each core site based on the P-wave and density data from the cores for the conversion of time to depth, and synthetic seismic sections from these data can be used as a correlation aid for the cores (e.g., Dal Forno & Gasperini 2008). The high-resolution profiles can be used to assist correlation of turbidite stratigraphy between local or distant sites as an independent measure of similarity (or not) of the shallow turbidite sections imaged at sites of interest. These data aid in the assessment of continuity of the turbidites between core sites and in unsampled locations and can extend to depths unreachable by coring techniques.

3.4.3. Evaluating correlations. Two classical approaches are commonly used in stratigraphic correlation. The simplest is visual, using corresponding remarkable features of multiple cores (e.g., Prell et al. 1986). Using this method, a skilled interpreter may ingest many disparate sources of information at a glance—including radiocarbon ages; grain size distributions; visible, CT, or X-ray imagery; and numerous geophysical/chemical wiggle traces—to develop the tie points for correlation. Alhough its simplicity is appealing, this method may give somewhat subjective results. The second method is to use a mathematical measure of the similarity between both signals (e.g., a correlation coefficient) and then optimize this measure when adjusting the age-depth relation (Martinson et al. 1987). This procedure gives a more objective result, but the fit is not always as good as with the simple visual correlation. A mathematical measure such as a correlation coefficient will indeed give more weight to the large timescale signal fluctuations (low-frequency variations), where much of the variance is located in the higher frequencies. With this method, the sharp events are not exactly in phase, as they should be according to the underlying simultaneity hypothesis. Although this second approach is therefore more objective, it can be less precise and, at present, is not capable of accounting for all data types simultaneously in the way that a human observer can.

Goldfinger et al. (2010) report detailed testing of correlation methods. The correlation of single events was done by calculating a Pearson correlation (parametric) coefficient and a Spearman rank (nonparametric) coefficient between events at multiple sites. The Pearson correlation coefficient is a measure of the relationship of two variables (in this case, two sites) obtained by dividing the covariance of the two variables by the product of their standard deviations (Cohen 1988). The Spearman rank coefficient is a measure of how one series varies relative to the other.

Figure 8

A turbidite pair (events 8 and 9) is correlated between three slope basin cores with unique sedimentary sources along the northern Sumatra margin. (*a*) Geophysical traces include gamma density, magnetic susceptibility, and computed tomography (CT) density. Cores are vertically aligned (flattened) to the basal contact for turbidite event 9. Calibrated ages are plotted at sample locations; the older age of event 9 in core 108PC is due to basal erosion, clearly visible in the CT data. The age of event 9 in core 104PC has a large error due to the small sample size. Events in 104 appear quite different than in the other two cores, with multiple thin coarse units attributed to retrogressive failure of a steep proximal slope. Core section breaks are shown in brown. (*b*) Core data are plotted against depth, with vertical scales flattened on the stratigraphic correlations in (*a*). Green tie lines show how data in (*a*) and (*b*) relate.

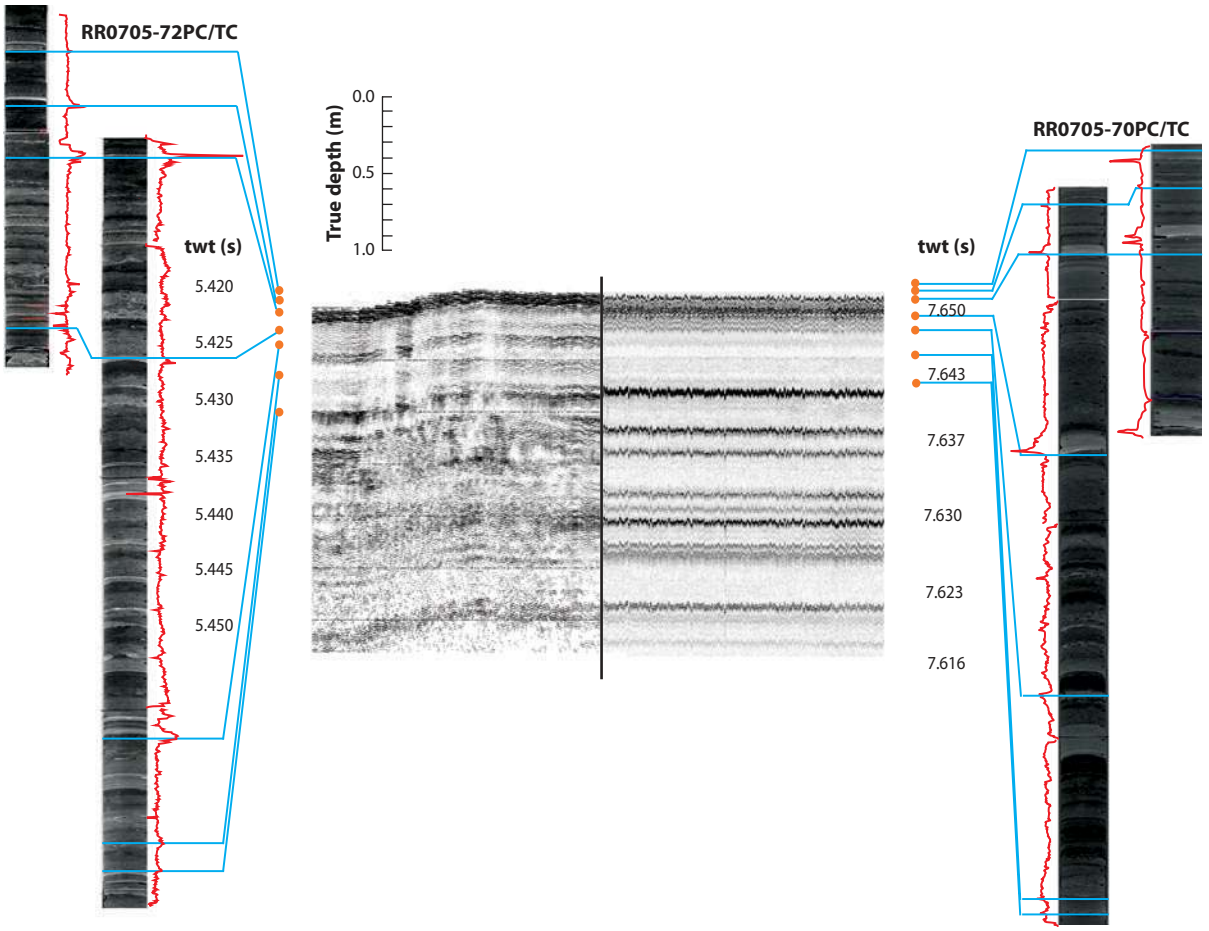

Figure 9

3.5 kHz Chirp records (sweep 2–6 kHz) from an outer slope basin at ~4,280 m (*left*) and a trench site at ~5,804 m (*right*), on the Sumatran margin west of the Pagai Islands. The Chirp records are correlated to the two corresponding piston cores. Typical underway record (*left*) and on-station 3.5 kHz data (*right*) are shown. The 3.5-kHz Chirp system can resolve objects ~20–30 cm apart, including the major turbidites, but cannot image the subevents or smaller turbidites. The two sites, separated by 81 km, have no sedimentological communication and correlate in their major stratigraphy and to the cores. CT imagery and magnetic susceptibility are shown.

They tested the use of least-squares search for optimal fit of stratigraphic sections represented by multiparameter physical property data. This method compares multiple fits and seeks those that minimize the difference between the tested pairs of traces. This method allows pure signal correlation, or allows input of key tie points such as known stratigraphic ties and recomputation of best fit and a transfer function based on the constrained data set (Hofmann et al. 2005). Multiple parameters and multiple cores were used, including P-wave amplitude, travel time, gamma density, and MS. This method closely mimics the process of visual correlation, adjusting the vertical scale of one core iteratively to match a reference core, thereby minimizing the distance between superimposed traces given known tie points.

Goldfinger et al. (2010) found no significant advantage to using signal processing methods over visual correlation. The assimilation of numerous data types, including CT, visible, and

X-ray imagery; visual core logs; and up to 6–8 geophysical/geochemical wiggle traces, is presently not possible with any algorithmic approach. A good stratigrapher has far greater computational capacity to assimilate disparate information and make informed interpretations of the data. The interpreter can interpret missing sections, core disturbances, data artifacts, and other anomalous stratigraphy and its possible causes and take these factors into account during the interpretation process.

3.4.4. Correlation of derivative parameters. To test the visual correlation series of Cascadia turbidites, Goldfinger et al. (2010) tested signal correlation between several derivative parameters from individual turbidites as numerical series down-core. The derivatives include turbidite mass, derived from the density records, and the number of coarse fraction units in each turbidite, which were compared between core sites along the Cascadia margin. Turbidite mass was estimated from the area under the gamma density plot.

For a vertical series of turbidites without a common origin, these parameters should be uncorrelated between remote sites. **Figure 10** shows correlation between multiple sites based on these parameters and reveals close correlations for both mass per event, and number of coarse fraction pulses per event. A consistent Pearson correlation coefficient of 0.93–0.96 for coarse pulse number per event was found for T1–T18 in JDF, Cascadia Hydrate Ridge, and Rogue channels. The Pearson correlation coefficient for mass per event is 0.72–0.87 for JDF and Cascadia channels, a moderately good correlation considering the large distance and wide variety of turbidite systems feeding into the two channels above their confluence (**Figure 6**). Correlation values were 0.68 for Hydrate Ridge, Cascadia, and JDF and 0.50–0.57 for the more complex and distant Rogue Channel (Goldfinger et al. 2010).

The close correlation of derivative parameters for the entire event series, along the length of the Cascadia margin, strongly supports a common origin and synchronous deposition, providing an independent test of earthquake origin.

3.5. Sedimentological and Mineralogical Characteristics

Investigators have attempted to distinguish seismically generated turbidites (seismo-turbidites) from storm, tsunami, and other deposits. Nakajima & Kanai (2000), Nakajima (2000), and Shiki et al. (1996, 2000a, 2000b) argue that seismo-turbidites may in some cases be distinguished sedimentologically. Shiki et al. (2000b) carefully examined known seismo-turbidites in Lake Biwa, Japan, including the AD 1185 Lake Biwa/Kyoto earthquake ($\sim M = 7.4$; Inouchi et al. 1996). These deposits are characterized by wide areal extent, multiple coarse-fraction pulses, variable mineralogical provenance (from multiple or line sources), and greater organic content, greater depositional mass, and coarser texture than the barely visible storm-generated events. Nakajima & Kanai (2000) observe that a known seismo-turbidite from the 1983 Japan Sea earthquake caused multiple slump events in many tributaries of a canyon system, resulting in multiple coarse sediment pulses. The stacked multipulsed turbidite subunits had distinct mineralogies and were found deposited in order of travel time to their lithologic sources, demonstrating synchronous triggering of multiple parts of the canyon system (Nakajima & Kanai 2000). Goldfinger et al. (2007) found a similar relationship with vertical stacking of separate mineralogic sources along the northern San Andreas fault (Goldfinger et al. 2008, Fig. 3 therein).

The Japanese investigators concluded, however, that defining the triggering mechanism even of known earthquake-related deposits was problematic in their studies, and that further study was needed. Gorsline et al. (2000) find that complexity, thickness, and areal extent also serve to distinguish Holocene seismo-turbidites in the Santa Monica and Alfonso basins of the California

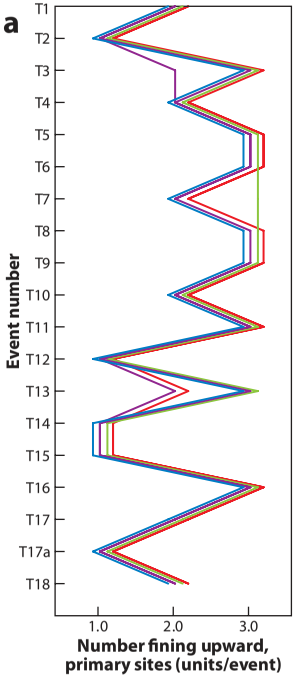

Number fining upward (units/event, primary sites)

	JDF	Casc.	HR	Rogue
T1	2	2	2	2
T2	1	1	1	1
T3	3	2	3	3
T4	2	2	2	2
T5	3	3	3	3
T6	3	3	3	3
T7	3	2	2	2
T8	3	3	3	3
T9	3	3	3	3
T10	2	2	2	2
T11	3	3	3	3
T12	1	1	1	1
T13	3	3	2	3
T14	1	1	1	1
T15	1	1	1	1
T16	3	3	3	3
T17	2	2	2	2
T17a	1	1	1	1
T18	2	2	2	2

	JDF	Casc.	HR	Rogue
JDF	1			
Casc.	0.92967	1		
HR	0.92967	0.915179	1	
Rogue	0.963406	0.961481	0.961481	1

Pearson coefficient (pulses/event)

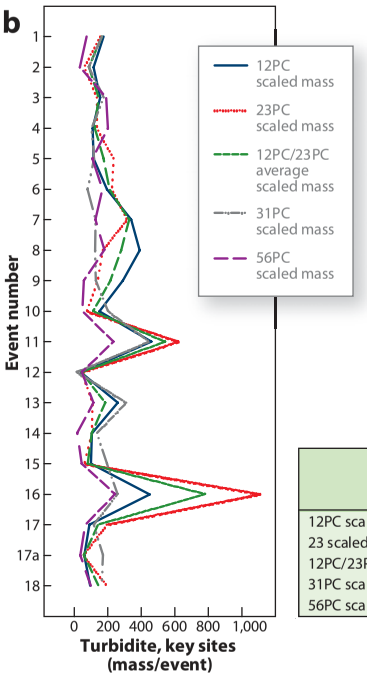

Turbidite number	12PC scaled mass	23PC scaled mass	12PC/23 avg. scaled mass	31PC scaled mass	56PC scaled mass
1	175	155	165	165	74
2	115	60	88	87	33
3	155	135	145	176	191
4	110	135	123	104	201
5	115	235	175	119	108
6	195	225	210	80	168
7	340	315	328	128	126
8	390	170	280	125	180
9	290	140	215	129	57
10	150	75	113	201	48
11	460	625	543	447	234
12	40	45	43	15	45
13	260	110	185	312	114
14	105	105	105	135	18
15	100	60	80	195	45
16	450	1110	780	258	243
17	90	195	143	117	66
17a	60	55	58	171	36
18	95				

	12PC scaled mass	23PC scaled mass	12PC and 32 avg. scaled mass	31PC scaled mass	56PC scaled mass
12PC scaled mass	1				
23 scaled mass	0.724113	1			
12PC/23PC avg. scaled mass	0.874762	0.967614	1		
31PC scaled mass	0.586783	0.505279	0.569769223	1	
56PC scaled mass	0.681114	0.683977	0.729845579	0.426721	1

Pearson coefficient (mass/event)

c

	23PC T3	23PC T4	23PC T5	23PC T6	23PC T7	23PC T8	23PC T9	23PC T10	23PC T11	23PC T12	23PC T13
12PC T3	0.7394	0.7765	0.8555	0.5660	0.0841	0.5790	0.5684	0.4228	0.6632	0.7481	0.4414
12PC T4	0.5599	0.7290	0.6260	0.6137	−0.0305	0.6000	0.4960	0.2750	0.6070	0.5730	0.4828
12PC T5	0.5393	0.7701	0.8010	0.4630	0.2079	0.2149	0.6604	0.6705	0.7680	0.5473	0.0028
12PC T6	0.3390	0.6400	0.4089	0.3277	−0.0325	0.0614	0.3643	0.3891	0.4111	0.1717	0.5003
12PC T7	0.8080	0.6674	0.5328	−0.0143	0.7786	−0.0728	0.3005	0.0456	0.1135	0.3903	0.2812
12PC T8	0.4256	0.2234	0.2276	−0.2901	0.7445	0.1667	0.1601	0.2036	−0.0716	0.2368	0.5345
12PC T9	0.4931	0.7050	0.6576	0.2648	−0.2524	0.4746	0.6100	0.0784	0.7797	−0.1748	0.2837
12PC T10	0.1580	−0.0378	0.5636	0.7427	−0.2168	0.7303	0.4836	0.7894	0.4770	0.6343	−0.1616
12PC T11	0.4769	0.6352	0.5957	0.5483	−0.2204	0.1846	0.7349	0.1713	0.8810	−0.2749	−0.0872
12PC T12	0.6994	0.4378	0.4748	0.3347	−0.3492	0.5236	0.3711	0.2778	0.2471	0.8241	−0.2210
12PC T13	0.1132	0.5389	0.3567	0.2467	−0.0551	0.4801	0.1384	−0.1150	0.4129	−0.0530	0.7731

borderland and Gulf of California, respectively. Gorsline et al. (2000) argued that reasonable estimates of discharge, sediment input, and source area may be used to constrain the sediment budget for flooding episodes. In this way, the upper bounds for nonseismic turbidites could be constrained. Goldfinger et al. (2010) suggest that deposition of seismic turbidites may not be governed directly by sediment supply, as they are triggered by ground failure and liquefaction and do not necessarily require a recharge of sediment supply between events. In Sumatra and Cascadia core sites, slope basin sites, and the Sumatran trench itself are presently isolated from modern sediment sources, thus turbidite deposition is almost entirely a result of recycling of older accreted materials.

3.6. Distinguishing Hyperpycnal Underflows and Storm Wave–Generated Turbidites

Globally, the depositional patterns of turbidites through time and space are highly site specific, responding to sediment supply, sea level, local morphology, earthquakes, and other forcings at specific times and places (Reeder 2002, Saller et al. 2004, Zühlsdorff et al. 2008), adding much complexity to the original sequence stratigraphic models (Vail et al. 1977, van Waggoner et al. 1990). However, the literature generally supports a model of higher turbidite frequency in deep water systems (abyssal) during sea-level lowstands and inactive systems during the Holocene (Shanmugam & Moiola 1982, Stow et al. 1985, Droz et al. 1996, Normark et al. 1997, Jorry et al. 2008); the reverse is common for carbonate platforms (i.e., Schlager et al. 1994). Highstand turbidites are far less common (Nelson 1968, Burke 1972, Zaragosi et al. 2000, Piper & Normark 2001, Khripounoff et al. 2003). Exceptions include systems with incised shelf canyons and shelf deltas that allow bypassing of the shelf and deep water turbidite deposition (i.e., Bengal Fan; Weber et al. 1997b), and very narrow shelves such as the Eel (Puig et al. 2003, 2004), Var (Mulder et al. 2003), and Monterey Canyon systems (Paull et al. 2005).

Evidence of hyperpycnal flows into lakes, shelf basins, and canyon heads is abundant; however, evidence of such flows transporting coarse material to abyssal depths is sparse. Most, if not all, examples involve short distances between the river mouth and canyon head, either during Pleistocene lowstand conditions, or in systems that have very narrow shelves during highstand conditions. Wright et al. (2001) observe that hyperpycnal flows are strongly affected by ambient currents and generally deliver sediment to the slope only upon relaxation of longshore currents, and similar observations have been made by other investigators (Sternberg 1986, Wheatcroft et al. 1997, Sommerfield & Nittrouer 1999, Wolf et al. 1999). Most investigators cite Pleistocene examples or examples with little or no shelf when referring to flows reaching the abyssal plain or lower

Figure 10

(*a*) Correlation of vertical series of coarse fraction pulses per turbidite for Juan de Fuca (JDF), Cascadia (Casc.), Hydrate Ridge (HR), and Rogue cores. Table and chart show the number of fining-upward coarse units per turbidite for events observed at all four sites. Correlation matrix shows the Pearson correlation coefficients for the four series. The four line plots are offset slightly for readability. The number of coarse pulses per event remains quite constant among widely separated core sites. (*b*) Correlation of turbidite mass for Cascadia, JDF channels, Hydrate Ridge, and Rogue Apron. Mass (dimensionless here) is derived from gamma density traces. (*c*) Pearson correlation coefficient for gamma density data for individual turbidites T3–T13 from JDF and Cascadia channels. This correlation is a numerical measure of the goodness of fit between the gamma density fingerprints among all turbidites at two sites. Green cells indicate those correlated visually and the best fit for ^{14}C data. Yellow cells are one turbidite above or below the best stratigraphic fit and are the only values that could be matches if one turbidite was miscorrelated. Remaining cells are unlikely fits given the stratigraphy and ^{14}C data. Orange cells are those that indicate a superior numerical fit but are an inferior fit based on visual correlation and ^{14}C data. Light green cells are those excluded by age data, though several are good numerical fits.

fan reaches (e.g., Normark et al. 1998, Piper et al. 1999, Mulder et al. 2003, Normark & Reid 2003). This is an expected result of the nearly direct connection between a river and canyon in the case of low sea level. Even systems that receive significant Holocene terrigenous input store sediment mostly in their upper reaches until something triggers further downslope movement (e.g., Johnson et al. 2005, Paull et al. 2005). During sea-level fluctuation, shelf width is commonly the primary control on canyon-channel system activity (e.g., Prins & Postma 2000, Covault et al. 2007).

Hyperpycnites are also commonly organic-rich as compared with seismic turbidites, having their sources in floods rather than in resuspension of older canyon wall material as in earthquake triggering (Shiki 1996, 2000b; Nakajima & Kanai 2000; Mulder et al. 2001). It has been suggested that this distinction may be used as a basis for distinguishing earthquake and storm deposits using optically stimulated luminescence (OSL) dating (Shirai et al. 2004). However, we suspect that this generalization may easily be violated as in the case of floods in very arid regions or earthquakes in heavily vegetated areas. For example, because the river drainage basins feeding Cascadia Basin are heavily vegetated, the Holocene turbidite tails linked to earthquake origins through a variety of methods (Goldfinger et al. 2008, 2010) are characterized by significant quantities of plant fragments (Nelson 1976).

Another point of confusion is the use of the term "deep water" in the literature. Some investigators use this term to describe sediment transport that reached the shelf edge, and others apply it to canyon head depths. For example, Hubbard (1992) reports removal of large quantities of sand into "deeper water" during a hurricane on St. Croix, though this is a local canyon head at 30-m depth, and still on the shelf. Ignition of turbidity currents requires greater vertical extent, and cannot be assumed simply by observation of sediment transport to canyon heads.

For active margin systems subject to wide continental shelves, or topographic barriers isolating the slope and abyssal plain, the turbidite record is more likely to contain an earthquake-dominated record (Nakajima & Kanai 2000; Abdeldayem et al. 2004; Goldfinger et al. 2008, 2010). Caution must be exercised to examine the river systems, their relationship to sea level during periods of interest, and the physiographic conditions of shelf width, forearc basins, and other barriers to hyperpycnal flow when evaluating a particular setting for turbidite paleoseismology.

3.6.1. Liquefaction due to wave loading. The passage of large waves, either via storms or tsunami, induces oscillatory fluctuation in the loading condition, as well as progressive increase in pore pressure after repeated wave cycles (e.g., Cheng et al. 2001). As successive waves pass, an undrained loading condition occurs, increasing pore fluid pressures and potentially bringing a slope closer to its static failure condition. Seed et al. (1988) report that a submarine landslide off the port of Nice, France, generated a tsunami that in turn triggered a slope failure by passage of the leading trough, which is believed to have occurred due to undrained flow liquefaction, and a 1–2% increase in shear stress caused by the passage of the wave. A more widespread deposit linked to a similar origin has been reported in the central Mediterranean, where a completely pelagic turbidite may have been triggered in deep water by a tsunami related to a volcanic eruption (Sironi & Rimoldi 2005). Another commonly cited example of wave loading in the literature is the failure of sediments around drilling platforms in the Mississippi Delta during Hurricane Camille in 1969 (Bea et al. 1983).

It is a matter of some debate as to the importance of this mechanism for slope failure even in shallow water. Chillarige et al. (1997) calculate that wave loading could not be the cause of observed sediment failures on the Frazier River delta, although spontaneous flow liquefaction there remains a poorly explained phenomenon possibly linked to free gas (Christian et al. 1997). Luternauer & Finn (1983) also conclude that wave loading does not cause sufficient sustained or transient pore pressure changes needed to initiate slope failure. Interestingly, cyclic loading can also strengthen

sediments that do not reach a failure criterion. Boulanger (2000) has shown through a series of cyclic loading and drainage tests, using an earthquake source rather than waves, that with a period of drainage between events, the void space decreased and shear strength increased from exposure to many cycles. Locat & Lee (2002) termed this condition "seismic strengthening" and suggest that it may explain the relative paucity of shallow landslides in Cascadia and elsewhere relative to passive margins (Lee et al. 2004). The same may well be true for periods of wave loading and draining periods between storms (Sassa et al. 2003; H. Lee, personal commununication) and has been modeled as resistance to liquefaction (Chang et al. 2004).

On the shelf near the uppermost Eel Canyon on the Cascadia margin, Puig et al. (2003, 2004) infer that fluidization in storm wave conditions is the likely cause of sediment fluid flows recorded at a study site in the Eel Canyon head in 120 m of water. They infer that shear failure erosion of the sediment (discussed below) is unlikely and that fluidization is a viable alternative. These authors cite the rapid development of sediment flows with increased wave height and conclude that the short time interval would be insufficient for erosive entrainment of material in the bottom boundary layer but is more consistent with the near instantaneous fluidization on arrival of storm waves.

3.6.2. Sediment erosion due to combined current and storm wave conditions. The potential for sediment erosion, given wave and current conditions, is commonly estimated by calculating wave orbital velocity and combining this with tidal or other current measurements or estimates to arrive at a combined estimate of shear stress in the bottom boundary layer (i.e., Madsen 1994). Puig et al. 2004 used this method to estimate the erosion potential in the head of Eel Canyon at 120-m water depth during two storms in January and March 2000. They calculate a shear stress of 0.17–0.2 Pa, 30 cm above the bottom, greater than the critical shear value of 0.07 for the top few centimeters of fluidized sediment but below the value of 0.27 Pa estimated for shallow subsurface sediments by Thomsen et al. 2002. They further conclude from this analysis that the observed sediment resuspension during the two storms is more likely due to sediment fluidization (as discussed above), because calculated shear stresses do not reach the critical value estimated for shallow sediments. Cheng et al. (1999), however, have shown that the calculations are highly dependent on the value of the roughness length of the seafloor (z0). Although the value of z0 is estimated or assumed as an input parameter to the frequently used shear stress calculations, it is also an unknown. This unknown value has been cited as a function of grain size, but various published rules of thumb vary over several orders of magnitude. As the calculation of near seabed shear stress is sensitive to this value, we conclude that explicit calculation of erosion potential is problematic without further detailed information about roughness of the seabed as well as further refinement of the techniques for calculating erosion potential.

Goldfinger et al. (2010) following Puig et al. (2004) calculate that maximum storm waves and tsunami both should have erosive power to a depth of ~450 m in Cascadia, including tidal down flow, or ~300 m from the waves alone. Larger values of z0, or consideration of bedforms or slopes, will increase this depth, as would adding the effects of the storm-driven, inshore Davidson Current. They conclude that such disturbances likely occur each winter season, though they apparently fail to ignite turbidity currents that reach the abyssal plain, where the most recent turbidite dates to the AD 1700 earthquake in nearly all localities.

4. DISCUSSION

It has become clear that an important consideration for investigations using turbidites to develop a paleoseismic record is an adequate number of samples and good areal coverage. The variability

of the turbidite record is typically not well known and becomes part of the investigation. In the case of sampling done in Cascadia, the NSAF, and Sumatra, the sample cruises were 30–45 sea days, and 80–110 new cores were collected in each case, along with ~60 older cores in Cascadia (Goldfinger et al. 2008, 2010; Patton et al. 2010). Part of the process includes determining which sites make good recorders of earthquakes, which do not, and which can best minimize or eliminate non-earthquake-sourced turbidity currents. Important to this is developing an understanding of the sensitivity of each site to the earthquake record. Sites that are too proximal may have gravel lag and missing sediment section, and distal sites may have thin mud turbidites and subdued log signatures. With only a few cores, it may be possible to develop a partial record, but broad areal sampling and replicate cores are required to establish robust interpretations, and provide multiple tests of earthquake origin, which may vary along the margin.

5. APPLICABILITY TO A VARIETY OF SETTINGS

As experience with marine paleoseismology has increased in recent years, so has the knowledge of what constitutes both favorable and unfavorable settings. Cascadia is now recognized as a highly favorable locality for the turbidite technique. It has a shallow plate dip, high sediment supply, and a filled trench that promotes development of fan systems and discrete channel systems leading away from the margin. These factors promote discrete monitoring of regions of the fault system by each channel system, and a high-resolution stratigraphic record. Cascadia is also located in a region of upwelling and high productivity. The hemipelagic sediment between turbidites is a mix of biogenic and extremely fine material from river plumes accumulating at a rate of ~1 m 10,000 y^{-1} in Cascadia Basin. This yields just enough datable material and separation between turbidites for good stratigraphic discrimination and correlation. Cascadia sites are also above the carbonate compensation depth (CCD), allowing good preservation of datable calcareous microfossils. Most of all, Cascadia has large-magnitude (estimated Mw = 9?) earthquakes with long enough recurrence times to allow accumulation of datable microfossils between most events. Cascadia also has both channel confluences for use as relative dating tests, and isolated slope basins for comparisons to other sites that are less isolated from other potential triggers of turbidity currents. The signal-to-noise ratio is important, and sites with very large earthquakes, a single simple fault system, and reduced input from other sources are factors that favor good preservation of an earthquake record.

Few other settings have as many favorable factors. For example, the northern San Andreas fault lies adjacent to a margin that shares many of the favorable conditions for turbidite distribution and dating found in Cascadia and has six channel confluences monitoring the fault between San Francisco and the Mendocino Triple Junction. However, the earthquake source is more distant, and earthquakes on the NSAF are smaller (maximum of Mw ~ 8, limited by crustal thickness). These factors and the lower sedimentation rates in northern California make the NSAF turbidite record more difficult to define than the Cascadia record.

In many subduction settings, favorable physiography is less common. In Sumatra, the trench is not filled, turbidity currents are directed southward into axial channel(s), and the trench depth ranges from 5,200–6,500 m, well below the CCD. There are no datable materials in the Sumatran trench. Globally, many trench systems are more similar to Sumatra than to Cascadia, so it is worth considering alternative strategies to deal with these issues. In Sumatra, well-selected slope basins are a reasonably good alternative. Slope basins are commonly relatively isolated and can be completely isolated from terrigenous sediment supply, as well as other slope basins and trench sites. They can be selected to be above the CCD, and in more productive shallower waters to

increase the sedimentation rate and provide datable microfossils. With dating and stratigraphic correlation, it is possible to link isolated sites and test for earthquake origin, mitigating the problem of axial trench sediment transport and lack of datable material. Stratigraphic correlation is quite effective even without datable material (Patton et al. 2010). Slope basins have one disadvantage: They are generally more proximal than the ideal. Experience in Cascadia has shown that 2–3 km of runout distance is adequate for turbidity currents to evolve from slump-debris flows, but slope basins may not be wide enough to accommodate the transition, requiring some trial-and-error sampling and sub-bottom surveying to select slope basin sites.

Another method of isolating core sites is used in the Iberian margin, where cores are separated by a bathymetric ridge, isolating sites from common sediment transport paths. These sites were ultimately correlated and used to develop a paleoseismic record of predecessor events to the 1755 Lisbon earthquake (Gracia et al. 2010).

In unfilled trenches, other factors may mitigate the problem of mixing in the axial channel. In Sumatra, for example, the trench is divided into compartments that do not communicate with each other by transverse fracture zones. This is also common in other trenches (Sak et al. 2009) and can be used to advantage in isolating segments of the margin, which may also be seismic segments.

6. FUTURE DIRECTIONS

The utility of turbidite stratigraphy has now allowed robust determination of long earthquake histories along the Cascadia margin and the northern San Andreas margin, and work is underway in Japan, Sumatra, and Patagonian and Alpine lakes and on the Southwest Iberian margin and elsewhere. Because marine sedimentation is continuous, along-strike stratigraphic correlation is possible, as well as the development of very long records critical to the understanding of plate boundary processes and earthquake probabilities.

In addition to dating past earthquakes and determining their rupture lengths, recent work suggests that more information may be available from the turbidite record. Goldfinger et al. (2007, 2008, 2010) note that the detailed structure of correlative turbidites shows consistency between isolated sites along the Cascadia and NSAF margins. Derivative parameters, including the relative mass, thickness, and number of coarse pulses of the turbidite series down core in separated and isolated sites, show surprising consistency. These factors form the basis for the success of the correlation methods based on physical property, but beyond that, they require further explanation. Goldfinger et al. (2010) note that the size and structure similarities are not correlated to factors such as the number of tributary canyons, or the long-term sediment supply, which is unlikely to change rapidly on such short timescales. They also note that sediment supply likely played little role in Cascadia during the Holocene, when most of the canyons were relict features. Goldfinger et al. (2008, 2010) suggest that, in Cascadia at least, the detailed correlations of the vertical structure of turbidites in widely separated sites isolated from each other imply more commonality to the deposits than just their synchronous deposition from a common source. They suggest that physiographic, oceanographic, or hydrodynamic controls fail to explain this consistency and propose that turbidites may be crude recorders of the original earthquake rupture sequence and that this may account for the regional consistency. Preliminary testing of this hypothesis has been done in the laboratory and using deposits from the NSAF 1906 and 2004 Sumatran earthquake and is at least permissive of such a connection (Goldfinger et al. 2010, Patton et al. 2010).

If correct, the implication is that first-order information on magnitude, rupture pattern, and perhaps directivity may be gleaned from turbidite records in mature studies with excellent spatial and temporal sampling of the stratigraphic record.

DISCLOSURE STATEMENT

The author is not aware of any affiliations, memberships, funding, or financial holdings that might be perceived as affecting the objectivity of this review.

LITERATURE CITED

Abdeldayem AL, Ikehara K, Yamazaki T. 2004. Flow path of the 1993 Hokkaido-Nansei-oki earthquake seismotrubidite, southern margin of the Japan Sea north basin, inferred from anisotropy of magnetic susceptibility. *Geophys. J. Int.* 157:15–24

Adams J. 1990. Paleoseismicity of the Cascadia subduction zone: evidence from turbidites off the Oregon-Washington margin. *Tectonics* 9:569–83

Anastasakis GC, Piper DJW. 1991. The character of seismo-turbidites in the S-1 sapropel, Zakinthos and Strofadhes basins, Greece. *Sedimentology* 38:717–33

Atwater BF, Hemphill-Haley E. 1997. Recurrence intervals for great earthquakes of the past 3,500 years at northeastern Willapa Bay, Washington. U.S. Geol. Surv. Prof. Pap., vol. 1576, 108 pp.

Atwater BF, Tuttle MP, Schweig ES, Rubin CM, Yamaguchi DK, Hemphill-Haley E. 2003. Earthquake recurrence inferred from paleoseismology. In *The Quaternary Period in the United States*, ed. AR Gillespie, SC Porter, BF Atwater, vol. 1, pp. 331–50. Amsterdam: Elsevier.

Azmon E. 1981. Use of clay fabric to distinguish turbidites from hemipelagic siltstone. *Sedimentology* 28:733–35

Bahk J-J, Han S-J, Khim B-K. 2004. Variations of terrigenous sediment supply to the southern slope of the Ulleung Basin, East/Japan Sea since the Last Glacial Maximum. *Geosci. J.* 8:381–90

Bea RG, Wright SG, Niedoroda AW. 1983. Wave-induced slides in South Pass Block 70, Mississippi Delta. *J. Geotech. Eng.* 109:619–44

Bernd Z, Jens M, Sjerry Van Der G, Jansen J, Rudolf N. 2002. Sediment logging techniques. In *Tracking Environmental Change Using Lake Sediments Basin Analysis, Coring, and Chronological Techniques*, ed. JP Smol, WM Last, HJB Birks, vol. 1, pp. 137–53. Netherlands: Springer

Biasi GP, Weldon RJ, Fumal TE, Seitz GG. 2002. Paleoseismic event dating and the conditional probability of large earthquakes on the southern San Andreas fault, California. *Bull. Seismol. Soc. Am.* 92:2761–81

Blaauw M, Heuvelink GBM, Mauquoy D, van der Plicht J, van Geel B. 2003. A numerical approach to ^{14}C wiggle-match dating of organic deposits: best fits and confidence intervals. *Quat. Sci. Rev.* 22:1485–500

Blais-Stevens A, Clague JJ. 2001. Paleoseismic signature in late Holocene sediment cores from Saanich Inlet, British Columbia. *Mar. Geol.* 175:131–48

Blumberg S, Lamy F, Arz HW, Echtler HP, Wiedicke M, et al. 2008. Turbiditic trench deposits at the South-Chilean active margin: A Pleistocene–Holocene record of climate and tectonics. *Earth Planet. Sci. Lett.* 268:526–39

Bondevik S, Mangerud J, Birks HH, Gulliksen S, Reimer P. 2006. Changes in North Atlantic radiocarbon reservoir ages during the Allerød and Younger Dryas. *Science* 312:1514–17

Boulanger E. 2000. Comportement cyclique des sédiments de la marge continentale de la rivière Eel: une explication possible pour le peu de glissements sous-marins superficiels dans cette region. MS thesis. Dept. Geol. and Geol. Eng., Laval Univ., Sainte-Foy, Quebec

Brunner CA, Ledbetter MT. 1987. Sedimentological and micropaleontological detection of turbidite muds in hemipelagic sequences: an example from the late Pleistocene levee of Monterey Fan, Central California continental margin. *Mar. Micropaleontol.* 12:223–39

Bryna P, Berg K, Forsberg CF, Solheim A, Kvalstada TJ. 2005. Explaining the Storegga Slide. *Mar. Pet. Geol.* 22:11–19

Burke K. 1972. Longshore drift, submarine canyons, and submarine fans in development of Niger delta. *AAPG Bull.* 56:1975–83

Chang CH, Chien LK, Chang YH. 2004. 3-D liquefaction potential analysis of seabed at nearshore area. *J. Mar. Sci. Tech.* 12:141–51

Chen Y, Hur H, Leigh J, Johnson A, Renambot L, et al. 2009. *The CoreWall Project—core visualization, stratigraphic correlation and rich media distribution*. Presented at workshop *The Future of Continental Scientific Drilling, a U.S. Perspective*, Denver, Colo.

Cheng LB, Sumer M, Freds J. 2001. Solutions of pore pressure build up due to progressive waves. *Int. J. Numer. Anal. Meth. Geomech.* 25:887–907
Cheng RT, Ling CH, Gartner JW. 1999. Estimates of bottom roughness length and bottom shear stress in South San Francisco Bay, California. *J. Geophys. Res.* 104:7715–28
Chillarige AV, Morgenstern NR, Robertson PK, Christian HA. 1997. Seabed instability due to flow liquefaction in the Fraser River Delta. *Can. Geotech. J.* 34:520–33
Christian HA, Woeller DJ, Robertson PK, Courtney RC. 1997. Site investigations to evaluate flow liquefaction slides at Sand Heads, Fraser River delta. *Can. Geotech. J.* 34:384–97
Cohen J. 1988. *Statistical Power Analysis for the Behavioral Sciences*. Hillsdale, NJ: Lawrence Erlbaum. 2nd. ed.
Covault JA, Normark WR, Romans BW, Graham SA. 2007. Highstand fans in the California borderland: the overlooked deep-water depositional systems. *Geology* 35:783–86
Dal Forno G, Gasperini L. 2008. ChirCor: a new tool for generating synthetic chirp-sonar seismograms. *Comput. Geosci.* 34:103–114
Droz L, Rigaut F, Cochonat P, Tofani R. 1996. Morphology and recent evolution of the Zaire turbidite system (Gulf of Guinea). *Geol. Soc. Am. Bull.* 108:253–69
Fairbanks RG, Mortlock RA, Chiu T-C, Cao L, Kaplan A, et al. 2005. Radiocarbon calibration curve spanning 0 to 50,000 years BP based on paired 230Th/234U/238U and 14C dates on pristine corals. *Quat. Sci. Rev.* 24:1781–96
Field ME. 1984. The submarine landslide of 1980 off northern California. *U.S. Geol. Surv. Circ.* 938:65–72
Field ME, Gardner JV, Jennings AE, Edwards BD. 1982. Earthquake induced sediment failures on a 0.25° slope, Klamath River Delta, California. *Geology* 10:542–46
Frappa M, Pujos M. 1994. Late Quaternary evolution of the French Guiana continental shelf-evidence from 3.5 kHz data. *Mar. Geol.* 121:231–45
Fukuma K. 1998. Origin and applications of whole-core magnetic susceptibility of sediments and volcanic rocks from Leg 152. *Proc. ODP Sci. Results* 152:271–80
Garfield N, Rago TA, Schnebele KJ, Collins CA. 1994. Evidence of a turbidity current in Monterey Submarine Canyon associated with the 1989 Loma Prieta earthquake. *Cont. Shelf Res.* 14:673–86
Goldfinger C, Grijalva K, Burgmann R, Morey AE, Johnson JE, et al. 2008. Late Holocene rupture of the northern San Andreas Fault and possible stress linkage to the Cascadia Subduction Zone. *Bull. Seismol. Soc. Am.* 98:861–89
Goldfinger C, Morey AE, Nelson CH, Gutierrez-Pastor J, Johnson JE, et al. 2007. Rupture lengths and temporal history of significant earthquakes on the offshore and north coast segments of the northern San Andreas Fault based on turbidite stratigraphy. *Earth Planet. Sci. Lett.* 254:9–27
Goldfinger C, Nelson CH, Johnson JE. 2003a. Deep-water turbidites as Holocene earthquake proxies: the Cascadia Subduction Zone and northern San Andreas Fault systems. *Annali Geofisica* 46:1169–94
Goldfinger C, Nelson CH, Johnson JE, Shipboard Scientific Party. 2003b. Holocene earthquake records from the Cascadia Subduction Zone and northern San Andreas Fault based on precise dating of offshore turbidites. *Annu. Rev. Earth Planet. Sci.* 31:555–77
Goldfinger C. 2009. Subaqueous paleoseismology. In *Paleoseismology*, ed. JP McAlpin, vol. 95, pp. 119–70. Amsterdam: Elsevier
Goldfinger C, Nelson CH, Morey A, Johnson JE, Gutierrez-Pastor J, et al. 2010. Turbidite event history: Methods and implications for Holocene paleoseismicity of the Cascadia Subduction Zone. USGS Professional Paper, U.S. Geological Survey, Reston, Va. 178 pp. **http://activetectonics.coas.oregonstate.edu/Goldfinger_1661.zip**
Gorsline DS, De Diego T, Nava-Sanchez EH. 2000. Seismically triggered turbidites in small margin basins: Alfonso Basin, Western Gulf of California and Santa Monica Basin, California Borderland. *Sediment. Geol.* 135:21–35
Gràcia E, Vizcaino A, Escutia C, Asiolic A, Garcia-Orellanad J, et al. 2010. Holocene earthquake record offshore Portugal (SW Iberia): applying turbidite paleoseismology in a slow-convergence margin. *Quat. Sci. Rev.* 29:1156–72
Grantz A, Phillips RL, Mullen MW, Starratt SW, Jones GA, Naidu AS. 1996. Character, paleoenvironment, rate of accumulation, and evidence for seismic triggering of Holocene turbidites, Canada Abyssal Plain, Arctic Ocean. *Mar. Geol.* 133:51–73

Gutierrez-Pastor J, Nelson CH, Goldfinger C, Johnson JE, Escutia C, et al. 2010. Earthquake control of Holocene turbidite frequency confirmed by hemipelagic sedimentation chronology on the Cascadia and northen California active continental margins. In *External Controls on Deep-Water Depositional Systems*, ed. B Kneller, B McCaffrey, OJ Martinsen. Soc. Sediment. Geol., Tulsa, Okla. Special publication. In press

Hagstrum JT, Atwater BF, Sherrod BL. 2004. Paleomagnetic correlation of late Holocene earthquakes among estuaries in Washington and Oregon. *Geochem., Geophys., Geosys.* 5:doi: 10.1029/2004GC000736

Hallett DJ, Hills LV, Clague JJ. 1997. New accelerator mass spectrometry radiocarbon ages for the Mazama tephra layer from Kootenay National Park, British Columbia, Canada. *Can. J. Earth Sci.* 34:1202–9

Heath MT. 2002. *Scientific Computing*. New York: McGraw-Hill. 563 pp.

Heezen BC, Ewing M. 1952. Turbidity currents and submarine slumps, and the 1929 Grand Banks earthquake. *Am. J. Sci.* 250:849–73

Hofmann DI, Fabian K, Schmieder F, Donner B, Bleil U. 2005. A stratigraphic network across the Subtropical Front in the central South Atlantic: multi-parameter correlation of magnetic susceptibility, density, X-ray fluorescence and d18O records. *Earth Planet. Sci. Lett.* 240:694–709

Hubbard DK. 1992. Hurricane-induced sediment transport in open-shelf tropical systems—an example from St. Croix, U.S. Virgin Islands. *J. Sediment. Petrol.* 62:946–60

Hughen KA, Baillie MGL, Bard E, Bayliss A, Beck JW, et al. 2004. Marine04 Marine radiocarbon age calibration, 26–0 ka BP. *Radiocarbon* 46:1059–86

Hughen KA, Lehman S, Southon J, Overpeck J, Marchal O, et al. 2006. Marine-derived 14C calibration and activity record for the past 50,000 years updated from the Cariaco Basin. *Quat. Sci. Rev.* 25:3216–27

Huh C-A, Su C-C, Wang C-H, Lee S-Y, Lin I-T. 2006. Sedimentation in the Southern Okinawa Trough—Rates, turbidites and a sediment budget. *Mar. Geol.* 231:129–39

Inouchi Y, Kinugasa Y, Kumon F, Nakano S, Yasumatsu S, Shiki T. 1996. Turbidites as records of intense palaeoearthquakes in Lake Biwa, Japan. *Sed. Geol.* 104:117–125

Iwaki H, Hayashida A, Kitada N, Ito H, Suwa S, Takemura K. 2003. Stratigraphic correlation of core samples from the Osaka Bay off Kobe based on magnetic properties and its implication for tectonic activity of the Osaka-wan fault for the last 6,300 years. *Eos Trans. AGU* 84(46), Fall Meet. Suppl., GP41C-0053 (Abstr.)

Jacoby GC, Bunker DE, Benson BE. 1997. Tree-ring evidence for an A.D. 1700 Cascadia earthquake in Washington and northern Oregon. *Geology* 25:999–1002

Johnson JE, Paull CK, Normark W, Ussler W. 2005. Late Holocene turbidity currents in Monterey Canyon and Fan Channel: implications for interpreting active margin turbidite records. *Eos Trans. AGU* 86(52), Fall Meet. Suppl., OS21A–1521 (Abstr.)

Jorry SJ, Droxler SW, Mallarino G, Dickens GR, Bentley SJ, et al. 2008. Bundled turbidite deposition in the central Pandora Trough (Gulf of Papua) since Last Glacial Maximum: linking sediment nature and accumulation to sea level fluctuations at millennial timescale. *J. Geophys. Res.* 113:1–15

Joseph LH, Rea DK, van der Pluijm BA. 1998. Use of grain size and magnetic fabric analyses to distinguish among depositional environments. *Paleoceanography* 13:491–501

Karlin RE, Abella SEB. 1992. Paleoearthquakes in the Puget Sound region recorded in sediments from Lake Washington, U.S.A. *Science* 258:1617–20

Karlin RE, Holmes M, Abella SEB, Sylwester R. 2004. Holocene landslides and a 3,500-year record of Pacific Northwest earthquakes from sediments in Lake Washington. *Geol. Soc. Am. Bull.* 116:94–108

Kastens KA. 1984. Earthquakes as a triggering mechanism for debris flows and turbidites on the Calabrian Ridge. *Mar. Geol.* 55:13–33

Kelsey HM, Nelson AR, Hemphill-Haley E, Witter RC. 2005. Tsunami history of an Oregon coastal lake reveals a 4,600 years record of great earthquakes on the Cascadia subduction zone. *GSA Bull.* 117:1009–32

Khripounoff A, Vangriesheim A, Babonneau N, Crassous P, Dennielou B, Savoye B. 2003. Direct observation of intense turbidity current activity in the Zaire submarine valley at 4,000 m water depth. *Mar. Geol.* 194:151–58

King J, Banerjee SK, Marvin J, Özdemir Ö. 1982. A comparison of different magnetic methods for determining the relative grain size of magnetite in natural materials: Some results from lake sediments. *Earth Planet. Sci. Lett.* 59:404–19

Kovanen DJ, Easterbrook DJ. 2002. Paleodeviations of radiocarbon marine reservoir values for the northeast Pacific. *Geology* 30:243–46

Lee HJ, Orzech K, Locat J, Konrad JM, Boulanger E. 2004. Seismic strengthening, a conditioning factor influencing submarine landslide development. *Proc. Can. Geotech. Conf.*, 57th, Quebec, pp. 8–14 [CD-ROM]

Locat J, Lee H. 2002. Submarine landslides: advances and challenges. *Can. Geotech. J.* 39:193–212

Lovlie R, Van Veen P. 1995. Magnetic susceptibility of a 180 m sediment core: reliability of incremental sampling and evidence for a relationship between susceptibility and gamma activity, pp. 258–66. In *Palaeomagnetic Applications in Hydrocarbon Exploration and Production*, ed. P Turner, A Turner, vol. 98. Geol. Soc., London

Luternauer J, Finn WDL. 1983. Stability of the Fraser River Delta front. *Can. Geotech. J.* 20:603–16

Madsen OS. 1994. Spectral wave-current bottom boundary layer flows. *Proc. Coast. Eng. Res. Counc./ASCE*, 24th, Kobe, Japan, pp. 384–98

Martinson DG, Pisias NG, Hays JD, Imbrie J, Moore TC Jr, Shackleton NJ. 1987. Age dating and orbital theory of ice ages: development of high-resolution 0 to 300,000-year chronostratigraphy. *Quat. Res.* 27:1–29

McCubbin DG. 1982. Barrier-island and strand-plain facies. In *Sandstone Depositional Environments*, Memoir no. 31, ed. PA Scholle, D Spearing, pp. 247–58. Am. Assoc. Petrol. Geol., Tulsa, Okla.

McHugh CMG, Seeber L, Cormier M-H, Dutton J, Cagatay N, et al. 2006. Submarine earthquake geology along the North Anatolia Fault in the Marmara Sea, Turkey: a model for transform basin sedimentation. *Earth Planet. Sci. Lett.* 248:661–84

Mulder T, Migeon S, Savoye B, Jouanneau JM. 2001. Twentieth century floods recorded in the deep Mediterranean sediments. *Geology* 29:1011–14

Mulder T, Syvitski JPM, Migeon S, Faugeres JC, Savoye B. 2003. Marine hyperpycnal flows; initiation, behavior and related deposits; a review. *Mar. Pet. Geol.* 20:861–82

Nakajima T. 2000. Initiation processes of turbidity currents; implications for assessments of recurrence intervals of offshore earthquakes using turbidites. *Bull. Geol. Surv. Jpn.* 51:79–87

Nakajima T, Kanai Y. 2000. Sedimentary features of seismoturbidites triggered by the 1983 and older historical earthquakes in the eastern margin of the Japan Sea. *Sediment. Geol.* 135:1–19

Nelson AR, Atwater BF, Bobrowsky PT, Bradley L-A, Clague JJ, et al. 1995. Radiocarbon evidence for extensive plate-boundary rupture about 300 years ago at the Cascadia subduction zone. *Nature* 378:371–74

Nelson AR, Kelsey HM, Witter RC. 2006. Great earthquakes of variable magnitude at the Cascadia subduction zone. *Quat. Res.* 65:354–65

Nelson AR, Sawai Y, Jennings AE, Bradley L, Gerson L, et al. 2008. Great-earthquake paleogeodesy and tsunamis of the past 2,000 years at Alsea Bay, central Oregon coast, USA. *Quat. Sci. Rev.* 27:747–68

Nelson CH. 1968. Marine geology of Astoria deep-sea fan. PhD thesis. Oregon State Univ., Corvallis. 289 pp.

Nelson CH. 1976. Late Pleistocene and Holocene depositional trends, processes, and history of Astoria deep-sea fan, northeast Pacific. *Mar. Geol.* 20:129–73

Niemi TM, Ben-Avraham Z. 1994. Evidence for Jericho earthquakes from slumped sediments of the Jordan River delta in the Dead Sea. *Geology* 22:395–98

Niklaus TR, Bonani G, Suter M, Wolfli W. 1994. Systematic investigation of uncertainties in radiocarbon dating due to fluctuations in the calibration curve. *Nucl. Instrum. Methods Phys. Res. B* 92:194–200

Nittrouer CA. 1978. Detrital sediment accumulation in a continental shelf environment of the Washington shelf. PhD thesis. Univ. Washington, Seattle

Noda A, TuZino T, Kanai Y, Furukawa R, Uchida J-I. 2008. Paleoseismicity along the southern Kuril Trench deduced from submarine-fan turbidites. *Mar. Geol.* 254:73–90

Normark WR, Damuth DE, Wickens HDV. 1997. Sedimentary facies and associated depositional elements of the Amazon fan. *Proc. Ocean Drill. Prog., Sci. Results* 155:611–51

Normark WR, Piper, Hiscott. 1998. Sea level controls on the textural characteristics and depositional architecture of the Hueneme and associated submarine fan systems, Santa Monica Basin, California. *Sedimentology* 45:53–70

Normark WR, Reid JA. 2003. Extensive deposits on the Pacific Plate from late Pleistocene North American glacial lake outbursts. *J. Geol.* 111:617–37

O'Brien NR, Nakazawa K, Tokuhashi S. 1980. Use of clay fabric to distinguish turbiditic and hemipelagic siltstones and silts. *Sedimentology* 27:47–61

Patton JR, Goldfinger C, Morey A, Erhardt M, Black B, Garrett AM, et al. 2010. Temporal clustering and recurrence of Holocene paleoearthquakes in the region of the 2004 Sumatra-Andaman earthquake. *Seismol. Res. Lett.* 81:290

Paull CK, Mitts P, Ussler W III, Keaten R, Greene HG. 2005. Trail of sand in upper Monterey Canyon: offshore California. *Geol. Soc. Am. Bull.* 117:1134–45

Piper DJW, Hiscott RN, Normark WR. 1999. Outcrop-scale acoustic facies analysis and latest Quaternary development of Hueneme and Dume submarine fans, offshore California. *Sedimentology* 46:47–78

Piper DJW, Normark WR. 2001. Sandy Fans-From Amazon to Hueneme and Beyond. *AAPG Bull.* 85:1407–38

Prell WL, Imbrie J, Martinson DG, Morley JJ, Pisias NG, et al. 1986. Graphic correlation of oxygen isotope stratigraphy: application to the late quaternary. *Paleoceanography* 1:137–62

Prins MA, Postma G. 2000. Effects of climate, sea level, and tectonics unraveled for last deglaciation turbidite records of the Arabian Sea. *Geology* 28:375–78

Puig P, Ogston AS, Mullenbach BL, Nittrouer CA, Sternberg RW. 2003. Shelf-to-canyon sediment-transport processes on the Eel continental margin (northern California). *Mar. Geol.* 193:129–49

Puig P, Ogston AS, Mullenbach BL, Nittrouer CA, Parsons JD, Sternberg RW. 2004. Storm-induced sediment gravity flows at the head of the Eel submarine canyon, northern California margin. *J. Geophys. Res.* 109:C03019

Puig P, Ogston AS, Mullenbach BL, Nittrouer CA, Sternberg RW. 2003. Shelf-to-canyon sediment-transport processes on the Eel continental margin (northern California). *Mar. Geol.* 193:129–49

Ramsey CB. 1995. Radiocarbon calibration and analysis of stratigraphy: the OxCal program. *Radiocarbon* 37:425–30

Ramsey CB. 2001. Development of the radiocarbon program OxCal. *Radiocarbon* 43:355–63

Reeder MS. 2002. Late Quaternary turbidite input into the east Mediterranean basin: new radiocarbon constraints on climate and sea-level control. *Geol. Soc. Lond. Spec. Publ.* 191:267–78

Robbins JA, Edgington DN. 1975. Determination of recent sedimentation rates in Lake Michigan using Pb-210 and Cs-137. *Geochim. Cosmochim. Acta* 39:285–304

Rogerson M, Weaver PPE, Rohling EJ, Lourens LJ, Murray JW, Hayes A. 2006. Color logging as a tool in high-resolution palaeoceanography. In *New Techniques in Sediment Core Analysis*, ed. RG Rothwell, FR Rack, pp. 99–112. Geol. Soc., London.

Ryan WBF, Heezen BC. 1965. Ionian Sea submarine canyons and the 1908 Messina turbidity current. *Geol. Soc. Am. Bull.* 76:915–32

Sak PB, Fisher DM, Gardner TW, Marshall JS, LaFemina PC. 2009. Rough crust subduction, forearc kinematics, and Quaternary uplift rates, Costa Rican segment of the Middle American Trench. *Geol. Soc. Am. Bull.* 121:992–1012

Saller AH, Noah JT, Ruzuar AP, Schneider R. 2004. Linked lowstand delta to basin-floor fan deposition, offshore Indonesia: an analog for deep-water reservoir systems. *AAPG Bull.* 88:21–46

Sassa S, Miyamoto J, Sekiguchi H. 2003. The dynamics of liquefied sediment flow undergoing solidification. In *Submarine Mass Movements and Their Consequences*, ed. J Locat, J Mienert, pp. 95–102. Nice, France: Kluwer

Satake K, Wang K, Atwater BF. 2003. Fault slip and seismic moment of the 1700 Cascadia earthquake inferred from Japanese tsunami descriptions. *J. Geophys. Res. B* 108:2325

Schimmelmann A, Lange CB, Roark B, Ingram L. 2006. Resources for paleoceanographic and paleoclimatic analysis: a 6,700-year stratigraphy and regional radiocarbon reservoir-age (1R) record based on varve counting and 14C-AMS dating for the Santa Barbara Basin, offshore California, U.S.A. *J. Sediment. Res.* 76:74–80

Schlager W, Reijmer J, Droxler A. 1994. Highstand shedding of carbonate platforms. *J. Sediment. Res.* 64B:270–81

Schnellmann M, Anselmetti FS, Giardini D, McKenzie JA, Ward SN. 2002. Prehistoric earthquake history revealed by lacustrine slump deposits. *Geology* 30:1131–34

Schuller P, Lovengreen CH, Handl J. 1993. 137Cs concentration in soil, prairie plants, and milk from sites in southern Chile. *Health Phys.* 64:157–61
Schuller P, Voigt G, Handl J, Ellies A, Oliva L. 2002. Global weapons' fallout 137Cs, in soils and transfer to vegetation in South-Central Chile. *J. Environ. Radioact.* 62:181–93
Seed HB, Seed RB, Schlosser F, Blondeau F, Juran I. 1988. The Landslide at the Port of Nice on October 16, 1979, Rep. no. EERC 88–10; Earthquake Eng. Res. Cent., Univ. of California, Berkeley
Shanmugam G, Moiola RJ. 1982. Eustatic control of turbidites and winnowed turbidites. *Geology* 10:231–35
Shiki T. 1996. Reading of the trigger records of sedimentary events—a problem for future studies. *Sediment. Geol.* 104:249–55
Shiki T, Cita MB, Gorsline DS. 2000a. Sedimentary features of seismites, seismo-turbidites and tsunamiites an introduction. *Sediment. Geol.* 135:7–9
Shiki T, Kumon F, Inouchi Y, Kontani Y, Sakamoto T, et al. 2000b. Sedimentary features of the seismo-turbidites, Lake Biwa, Japan. *Sediment. Geol.* 135:37–50
Shirai M, Tsukamoto S, Ujiie Y, Komatsubara J, Kondo R, et al. 2004. A possibility of OSL-dating as an indicator of transportation history of turbidites. Am. Geophys Union, Washington, DC. Fall Meet. Abstr., p. C1370
Sironi M, Rimoldi B. 2005. Prehistoric mega-tsunami in the eastern Mediterranean and its sedimentary response. *Rendiconti Lincei* 16:137–57
Solheim A, Bryn P, Sejrup HP, Mienert J, Berg K. 2005. Ormen Lange—an integrated study for the safe development of a deep-water gas field within the Storegga Slide Complex, NE Atlantic continental margin; executive summary. *Mar. Pet. Geol.* 22:1–9
Sommerfield CK, Nittrouer CA. 1999. Modern accumulation rates and a sediment budget for the Eel shelf: a flood-dominated depositional environment. *Mar. Geol.* 154:227–41
St. Onge G, Mulder T, Piper DJW, Hillaire-Marcel C, Stoner JS. 2004. Earthquake and flood-induced turbidites in the Saguenay Fjord (Québec): a Holocene paleoseismicity record. *Quat. Sci. Rev.* 23:283–94
Stacey MW, Brown AJ. 1988. Vertical structure of density and turbidity currents: theory and observations. *J. Geophys. Res.* 93:3528–42
Sternberg RW. 1986. Transport and accumulation of river-derived sediment on the Washington continental shelf, USA. *J. Geol. Soc. Lond.* 143:945–56
Stow DAV, Howell DG, Nelson CH. 1985. Sedimentary, tectonic, and sea-level controls. In *Submarine Fans and Related Turbidite Systems*, ed. Bouma AH, Normark WR, Barnes NE, pp 15–22. Berlin: Springer
Stupavsky M, Gravenor CP, Dumala R. 1976. Technique for measurement of isotropic magnetic susceptibility of till. *Geol. Soc. Am. Bull.* 87:818–20
Stuvier M, Reimer PJ, Bard E, Beck JW, Burr GS, et al. 1998. INTCAL98 Radiocarbon age calibration 24,000-0 cal BP. *Radiocarbon* 40:1041–83
Telford RJ, Heegaard E, Birks HJB. 2004. The intercept is a poor estimate of a calibrated radiocarbon age. *The Holocene* 14:296–98
Thomsen L, van Weeringm T, Gust G. 2002. Benthic boundary layer characteristics at the Iberian continental margin. *Progr. Oceanogr.* 52:315–29
Thomson J, Colley JS, Weaver PPE. 1988. Bioturbation into a recently emplaced deep-sea turbidite as revealed by 210Pb excess, 230Th excess and planktonic Foraminifera distributions. *Earth Planet. Sci. Lett.* 90:157–73
Thomson J, Weaver PPE. 1994. An AMS radiocarbon method to determine the emplacement time of recent deep-sea turbidites. *Sed. Geol.* 89:1–7
Vail PR, Mitchum RMJ, Todd RG, Widmier JM, Thompson SI, et al. 1977. Seismic stratigraphy and global changes in sea level. In *Seismic Stratigraphy—Application to Hydrocarbon Exploration*, *Volume Memoir 26*, ed. CE Payton, pp. 49–212. Am. Assoc. Pet. Geol., Tulsa, Okla.
Van Wagoner JC, Mitchum RM, Campion KM, Rahmanian VD. 1990. *Siliciclastic Sequence Stratigraphy in Well Logs, Cores and Outcrops*. Methods Explor. Ser. no. 7. Am. Assoc. Pet. Geol., Tulsa, Okla. 55 pp.
Völker D, Reichel T, Wiedicke M, Heubeck C. 2008. Turbidites deposited on Southern Central Chilean seamounts: evidence for energetic turbidity currents. *Mar. Geol.* 251:15–31
Walanus A. 2008. Drawing the optimal depth-age curve on the basis of calibrated radiocarbon dates. *Geochronometria* 31:1–5

Waldmann N, Ariztegui D, Anselmetti FS, Austin JJA, Dunbar R, et al. 2008. Seismic stratigraphy of Lago Fagnano sediments (Tierra del Fuego, Argentina)—a potencial archive of Paleoclimatic change and tectonic activity since the Late Glacial. *Geologica Acta* 6:101–10

Weber ME, Niessen F, Kuhn G, Wiedicke M. 1997a. Calibration and application of marine sedimentary physical properties using a multi-sensor core logger. *Mar. Geol.* 136:151–72

Weber ME, Wiedicke MH, Kudrass HR, Hübscher C, Erlenkeuser H. 1997b. Active growth of the Bengal Fan during sea-level rise and highstand. *Geology* 25:315–18

Wheatcroft RA. 1992. Experimental tests for particle size-dependent bioturbation in the deep ocean. *Limnol. Oceanogr.* 37:90–104

Wheatcroft RA, Sommerfield CK, Drake DE, Borgeld J, Nittrouer CA. 1997. Rapid and widespread dispersal of flood sediment on the northern California margin. *Geology* 25:163–66

Wolf SC, Nelson CH, Hamer MR, Dunhill G, Phillips RL. 1999. The Washington and Oregon mid-shelf silt deposit and its relation to the late Holocene Columbia River sediment budget. Open File Rep. 99–173. U.S. Geolog. Surv., Washington, DC

Wright LD, Friedrichs CT, Kim SC, Scully ME. 2001. Effects of ambient currents and waves on gravity-driven sediment transport on continental shelves. *Mar. Geol.* 175:25–45

Zaragosi S, Auffret GA, Faugeres J-C, Garlan T, Pujol C, Cortijo E. 2000. Physiography and recent sediment distribution of the Celtic deep-sea fan, Bay of Biscay. *Mar. Geol.* 169:207–37

Zdanowicz CM, Zielinski GA, Germani MS. 1999. Mount Mazama eruption: Calendrical age verified and atmospheric impact assessed. *Geology* 27:621–24

Zühlsdorff C, Hanebuth TJJ, Henrich R. 2008. Persistent quasi-periodic turbidite activity off Saharan Africa and its comparability to orbital and climate cyclicities. *Geo-Marine Lett.* 28:87–95

Annual Review of
Marine Science

Volume 3, 2011

Contents

Errata

An online log of corrections to *Annual Review of Marine Science* articles may be found at http://marine.annualreviews.org/errata.shtml